

JGR Atmospheres



RESEARCH ARTICLE

10.1029/2024JD040877

Key Points:

- 8-hr ozone concentrations frequently exceed 70 parts per billion by volume at Carlsbad Caverns National Park
- A box modeling analysis indicates that local ozone production is most sensitive to nitrogen oxide levels
- A subset of high ozone days was influenced by photochemically aged air masses carrying ozone from upwind oil and gas production regions

Supporting Information:

Supporting Information may be found in the online version of this article.

Correspondence to:

J. L. Collett Jr.,
Jeffrey.Collett@colostate.edu

Citation:

Marsavin, A., Pan, D., Pollack, I. B., Zhou, Y., Sullivan, A. P., Naimie, L. E., et al. (2024). Summertime ozone production at Carlsbad Caverns National Park, New Mexico: Influence of oil and natural gas development. *Journal of Geophysical Research: Atmospheres*, 129, e2024JD040877. <https://doi.org/10.1029/2024JD040877>






Received 25 JAN 2024

Accepted 16 JUN 2024

Author Contributions:

Conceptualization: Emily V. Fischer, Anthony J. Prenni, Bret A. Schichtel, Barkley C. Sive, Jeffrey L. Collett Jr.
Data curation: Da Pan, Ilana B. Pollack, Yong Zhou, Amy P. Sullivan, Barkley C. Sive, Jeffrey L. Collett Jr.
Formal analysis: Andrey Marsavin
Funding acquisition: Emily V. Fischer, Anthony J. Prenni, Jeffrey L. Collett Jr.
Investigation: Andrey Marsavin

Summertime Ozone Production at Carlsbad Caverns National Park, New Mexico: Influence of Oil and Natural Gas Development

Andrey Marsavin¹ , Da Pan¹, Ilana B. Pollack¹, Yong Zhou¹, Amy P. Sullivan¹, Lillian E. Naimie¹, Katherine B. Benedict^{1,2}, Julieta F. Juncosa Calahoranno¹, Emily V. Fischer¹, Anthony J. Prenni^{3,4} , Bret A. Schichtel^{3,4} , Barkley C. Sive³ , and Jeffrey L. Collett Jr.¹ 

¹Department of Atmospheric Science, Colorado State University, Fort Collins, CO, USA, ²Now at Earth and Environmental Science, Los Alamos National Laboratory, Los Alamos, NM, USA, ³Cooperative Institute for Research in the Atmosphere, Colorado State University, Fort Collins, CO, USA, ⁴US National Park Service, Air Resource Division, Lakewood, CO, USA

Abstract Southeastern New Mexico's Carlsbad Caverns National Park (CAVE) has increasingly experienced summertime ozone (O_3) exceeding an 8-hr average of 70 parts per billion by volume (ppbv). The park is located in the western part of the Permian oil and natural gas (O&G) basin, where production rates have increased fivefold in the last decade. We investigate O_3 –precursor relationships by constraining the F0AM box model to observations of nitrogen oxides ($NO_x = NO + NO_2$) and a suite of volatile organic compounds (VOCs) collected at CAVE during summer 2019. O&G-related VOCs dominated the calculated VOC reactivity with hydroxyl radicals (OH) on days when O_3 concentrations were primarily controlled by local photochemistry. Radical budget analysis showed that NO_x levels were high enough to impose VOC sensitivity on O_3 production in the morning hours, while subsequent NO_x loss through photochemical consumption led to NO_x -sensitive conditions in the afternoon. Maximum daily O_3 was responsive to both NO_x and O&G-related VOC reductions, with NO_x reductions proving most effective. The model underestimated observed O_3 during a 5-day high O_3 episode that was influenced by photochemically aged O&G emissions, as indicated by back-trajectory analysis, low *i*-/*n*-pentane ratios, enhanced secondary VOCs, and low ratios of NO_x to total reactive oxidized nitrogen (NO_y). Model-observation agreement was improved by constraining model NO_x with observed NO_y , which approximates NO_x at the time of emission, indicating that a large fraction of O_3 during this episode was formed nonlocally.

Plain Language Summary New Mexico's Carlsbad Caverns National Park has faced an increase in ground-level ozone pollution. Summertime southeasterly winds place the park directly downwind of the Permian basin, one of the largest and most productive oil and natural gas (O&G) basins in the US. Our study, conducted using measurements collected in the park during summer 2019 and an air quality model, investigates how emissions from O&G activities affect ozone production. We find that local ozone production is sensitive to changes in both nitrogen oxides and volatile organic compound levels, but more significant reductions in ozone can be achieved by preferentially lowering nitrogen oxides. While the Permian is the closest O&G basin to the park, controlling ozone pollution may require emission reductions from other basins and shale plays in the region, as the park is sometimes impacted by aged air masses that transport ozone from farther upwind.

1. Introduction

Tropospheric ozone (O_3) is a secondary air pollutant associated with adverse effects on both human and ecosystem health (Cohen et al., 2017; Kohut, 2007; Monks et al., 2015). O_3 was designated as a criteria pollutant by the US Environmental Protection Agency (EPA) following requirements set out under the 1970 Clean Air Act and subsequent amendments. Over the last 20 years, targeted reductions in emissions of nitrogen oxides ($NO_x = NO + NO_2$) and volatile organic compounds (VOCs)—precursors to O_3 formation—have led to a steady decline in maximum daily 8-hr average (MDA8) O_3 across much of the US (Gaudel et al., 2018; Simon et al., 2015). However, certain regions, particularly in the western and central US, have seen more modest declines or even increasing O_3 trends (Strode et al., 2015; US EPA, 2023). Sources of O_3 precursors that have gained prominence or recognition in recent years include enhanced wildfire activity (Jaffe et al., 2022), volatile chemical

© 2024 Los Alamos National Laboratory and The Author(s). This article has been contributed to by U.S. Government employees and their work is in the public domain in the USA.

This is an open access article under the terms of the [Creative Commons Attribution-NonCommercial License](https://creativecommons.org/licenses/by-nc/4.0/), which permits use, distribution and reproduction in any medium, provided the original work is properly cited and is not used for commercial purposes.

Methodology: Andrey Marsavin, Da Pan, Ilana B. Pollack, Yong Zhou, Amy P. Sullivan, Lillian E. Naimie, Katherine B. Benedict, Julieta F. Juncosa Calahoranno, Emily V. Fischer, Anthony J. Prenni, Bret A. Schichtel, Barkley C. Sive, Jeffrey L. Collett Jr.

Project administration: Emily V. Fischer, Anthony J. Prenni, Bret A. Schichtel, Barkley C. Sive, Jeffrey L. Collett Jr.

Resources: Da Pan, Ilana B. Pollack, Yong Zhou, Emily V. Fischer, Anthony J. Prenni, Barkley C. Sive, Jeffrey L. Collett Jr.

Supervision: Emily V. Fischer, Anthony J. Prenni, Barkley C. Sive, Jeffrey L. Collett Jr.

Validation: Da Pan, Ilana B. Pollack, Yong Zhou, Amy P. Sullivan, Lillian E. Naimie, Katherine B. Benedict, Julieta F. Juncosa Calahoranno, Emily V. Fischer, Anthony J. Prenni, Bret A. Schichtel, Barkley C. Sive, Jeffrey L. Collett Jr.

Visualization: Andrey Marsavin
Writing – original draft: Andrey Marsavin

Writing – review & editing: Da Pan, Ilana B. Pollack, Yong Zhou, Amy P. Sullivan, Lillian E. Naimie, Katherine B. Benedict, Julieta F. Juncosa Calahoranno, Emily V. Fischer, Anthony J. Prenni, Bret A. Schichtel, Barkley C. Sive, Jeffrey L. Collett Jr.

product emissions (Coggon et al., 2021; Seltzer et al., 2022), and the oil and natural gas (O&G) industry (Allen, 2016; Pozzer et al., 2020; Tzompa-Sosa & Fischer, 2021).

Since the early 2010s, the US has emerged as the world's largest producer of O&G, largely due to the widespread adoption of horizontal drilling and improved hydraulic fracturing technologies (US EIA, 2021). Air pollutant emissions from O&G activities have also increased: satellite observations show rising NO₂ tropospheric columns over several US O&G production regions (Bakken, Eagle Ford, and Permian basins), in contrast to declining NO₂ over major urban regions (Dix et al., 2020; Majid et al., 2017). Satellite observations have also revealed recent (e.g., 2017–2019) increases in methane (CH₄) emissions from US O&G basins, which correlate with rising O&G production rates, active well counts, and new well drilling activities (Lu et al., 2023). These top-down CH₄ emission estimates are much larger than reported in emission inventories, suggesting that emissions of other VOCs are likely also underestimated (Dalsøren et al., 2018; Francoeur et al., 2021; Kort et al., 2016; Li et al., 2017).

Many of the largest O&G basins in the US are in proximity to national parks, including those designated as federal Class I areas protected under the Clean Air Act (Benedict et al., 2019, 2020; Naimie et al., 2022; Prenni et al., 2016). In recent years, O₃ measured at New Mexico's Carlsbad Caverns National Park (CAVE) has consistently exceeded the EPA's National Ambient Air Quality Standards (NAAQS), with the 3-year running average of the annual 4th highest MDA8 O₃ surpassing 70 ppbv each year since 2018. This increase in O₃ at CAVE coincides with a surge in O&G production from the nearby Permian basin, the largest oil-producing and second-largest natural gas-producing basin in the US (Robertson et al., 2020). O&G production in the Permian has increased by a factor of 5 between 2012 and 2022, with daily production exceeding 5 million barrels of oil and 600 million m³ of natural gas as of October 2023 (US EIA, 2023). Other O&G basins in the region, including Oklahoma's Anadarko basin and south Texas' Eagle Ford shale play, have also experienced increases in O&G production. However, the combined production from the Anadarko and Eagle Ford areas amounts to less than 30% of oil and 60% of natural gas production from the Permian (US EIA, 2023).

The ~160,000 km² Permian basin is divided into two major sub-basins of roughly similar size: the Delaware basin to the west (nearest to CAVE) and the Midland basin to the east (Figure 1). NO_x emitted from the two sub-basins originate from engines used in various O&G equipment (e.g., drill rigs, pump jacks, compressors), natural gas processing plants, gas flares, as well as from roads and small towns interspersed among the region (Dix et al., 2022; Francoeur et al., 2021; Gorchov Negron et al., 2018). The Midland sub-basin has a higher fraction of urban NO_x emissions due to the presence of the Midland–Odessa metro area (population: ~300,000), ~200 km east of CAVE (Dix et al., 2022). VOC emissions result from the venting of petroleum hydrocarbons, volatilization of hydrocarbon-based drilling fluids, and incomplete combustion of fuels used in O&G equipment (Dix et al., 2023; Francoeur et al., 2021; Ku et al., 2024). Summertime easterly winds can transport these emissions to the west of the primary source regions (Barkley et al., 2023; Crosman, 2021; Dix et al., 2023). Consequently, concentrations of VOCs commonly associated with O&G (e.g., light alkanes) are ~1 order of magnitude greater at CAVE than at other southwestern US national parks (Benedict et al., 2020).

O₃ in the troposphere is formed through a set of nonlinear photochemical reactions involving NO_x, VOCs, and free radical species. While the photolysis of NO₂ directly leads to O₃ production, peroxy radicals (sourced from VOC oxidation) are needed to regenerate NO₂ from NO, completing the O₃ production cycle (Chameides & Walker, 1973; Sillman et al., 1990). The rate of O₃ production increases with NO_x concentration in low-NO_x environments (NO_x-sensitive regime), but may decrease if NO_x levels are high enough to act as a net radical sink (VOC-sensitive regime). O₃ production near the transition between these two regimes can be sensitive to both NO_x and VOCs (Sillman & He, 2002; P. Wang et al., 2019). Identifying the dominant photochemical regime at a given location is a key step toward optimizing O₃ control strategies. Recent fuel-based estimates have suggested that VOC/NO_x emission ratios from O&G activities are significantly underestimated by the US EPA's National Emissions Inventory (NEI), which affects how O₃ production downwind of O&G basins is represented in chemical transport models (Francoeur et al., 2021). In situ measurements of O₃ precursors are therefore needed to complement bottom-up emission inventory estimates and to assess the contributions of various emissions sources to O₃ production at receptor sites like CAVE.

During the summer of 2019, O₃ and a large suite of its precursors were measured at CAVE as part of the Carlsbad Caverns Air Quality Study (CarCavAQS). Pan et al. (2023) characterized the sources of VOCs impacting CAVE during this study period using positive matrix factorization (PMF). Seven VOC source factors were identified,

including three that were linked to primary O&G emissions, two linked to secondary chemical production, one associated with C_2 - C_4 alkenes, and one related to the regional background. Pollack et al. (2023) used this source apportionment, together with observations of NO_x and peroxy acyl nitrates (PANs), to demonstrate that emissions from O&G activities were the primary drivers of local photochemistry, with consistently high VOC/NO_x ratios implying NO_x -sensitive O_3 production. These studies motivated a detailed model analysis of O_3 production at CAVE, offering a comparison to prior observational insights.

We present results from a zero-dimensional (0-D) “box” model constrained to CarCavAQS observations. Box models can effectively simulate radical chemistry with detailed chemical mechanisms and observational constraints, avoiding uncertainties stemming from emission inventories (Cardelino & Chameides, 1995; Kim et al., 2022). These advantages come at the cost of a simplified parameterization of physical processes such as advection and entrainment. Box models have been previously used alongside field observations to study O_3 production within or near O&G basins, including the Upper Green River (Carter & Seinfeld, 2012), Uinta (Edwards et al., 2013, 2014), and Denver-Julesburg basins (Lindaas et al., 2019; McDuffie et al., 2016) in the US, as well as the Yellow River delta in China (Chen et al., 2020; Lee et al., 2021). The current study represents the first box model analysis constrained to ground-based O_3 precursor observations downwind of the Permian basin. We identify key factors driving day-to-day variability in O_3 at CAVE and use the model to assess the impact of potential changes in NO_x and VOC emissions on O_3 production.

2. Methods

2.1. CarCavAQS Measurements and VOC Source Apportionment

CarCavAQS was conducted between 7/25 and 9/5/2019. This work will focus on the 35-day period (7/30–9/2) during which speciated VOC measurements were available. The sampling site and meteorological conditions during the study are detailed by Naimie et al. (2022), Pan et al. (2023), and Pollack et al. (2023). Briefly, measurements were made from the CAVE Biology Building (32.18°N, 104.44°W; 1,335 m elevation), with

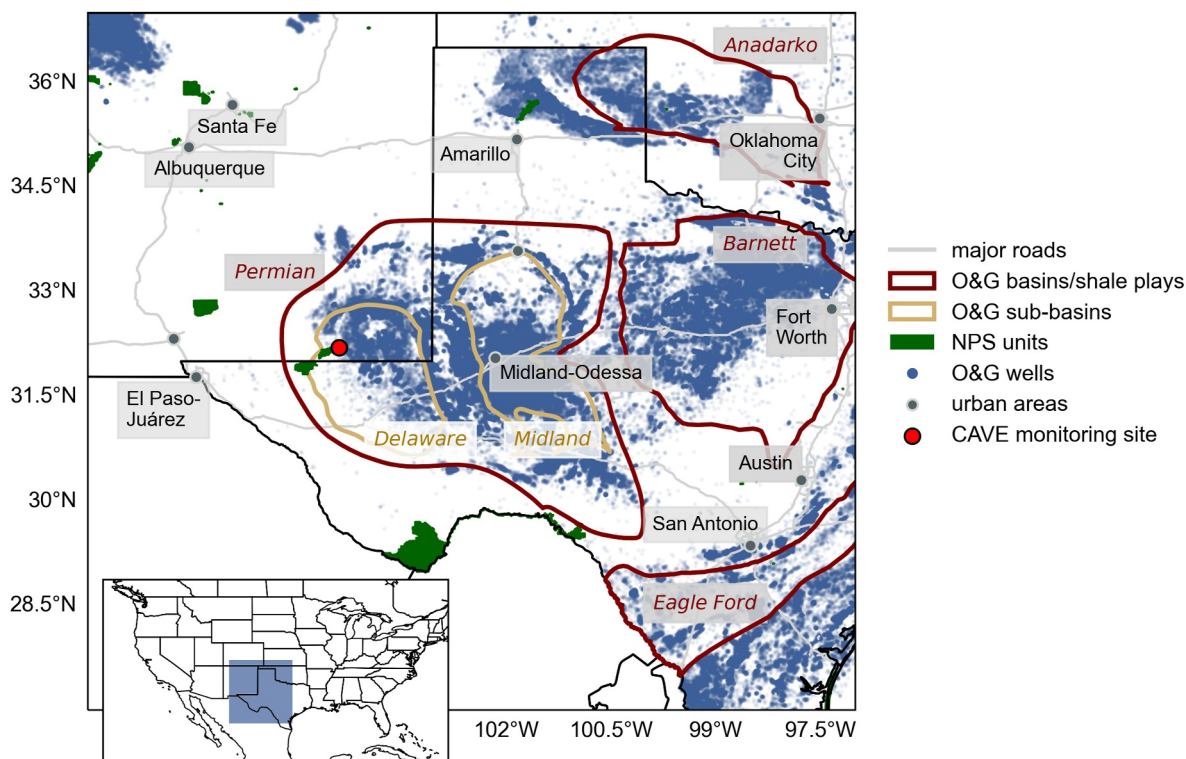


Figure 1. Map of study region showing the CAVE monitoring site, active O&G wells (HIFLD, 2019), other National Park Service (NPS) units, major roads, urban areas, and outlines of key O&G basins/shale plays (US EIA, 2016). The Delaware and Midland sub-basins are outlined within the Permian basin.

instrument inlets positioned 6–7 m above ground level. The site sits on a ridge near the northwestern corner of the Permian basin, ~300 m in prominence above the basin floor.

VOC measurements from the following instruments are used in this work:

- C_2 – C_{10} hydrocarbons, C_1 – C_2 halocarbons, and C_1 – C_5 alkyl nitrates ($RONO_2$) were measured with a custom automated 5-channel, 3-gas chromatograph (GC) analytical system with mass spectrometric, flame ionization, and electron capture detectors (Abeleira et al., 2017; Benedict et al., 2019; Pan et al., 2023; Sive et al., 2005).
- Isoprene, acetonitrile, and select oxidized VOCs (OVOCs; acetone, acetaldehyde, methyl ethyl ketone (MEK), and methyl vinyl ketone (MVK)) were measured with a quadrupole proton transfer reaction-mass spectrometer (PTR-MS; PTR-MS HS, Ionicon Analytik; Pan et al., 2023).
- Peroxyacetyl nitrate (PAN) and peroxypropionyl nitrate (PPN) were measured with a custom gas chromatograph-electron capture detector (GC-ECD; Pollack et al., 2023).
- C_1 – C_7 carbonyl compounds were measured by adsorption from ambient air in 2,4-dinitrophenylhydrazine (DNPH)-coated sorbent cartridges (Waters Sep-Pak). Cartridges were collected once per day from 10:00 to 17:00 local time (LT) at a flow rate of 1.5 L min^{-1} , downstream of an O_3 scrubber. After the campaign, the cartridges were extracted with acetonitrile and resulting samples analyzed with high-performance liquid chromatography with ultraviolet (UV) detection (HPLC-UV; Fedak et al., 2018).

Details regarding instrument operation, including calibration procedures, measurement precision, and method detection limits (MDLs), are provided in the cited references. Data from all VOC instruments except for the carbonyl cartridges were averaged to 1-hr intervals to match the sampling frequency of the 5-channel GC system. All VOCs measured at 1-hr resolution are listed in Table S1 of the Supporting Information S1.

O_3 was measured with a Thermo 49i UV absorption analyzer. Prior studies have shown that UV absorption analyzers can be prone to positive interference when sampling biomass burning smoke (Bernays et al., 2022; Long et al., 2021) or industrial plumes rich in VOCs with strong absorption cross sections in the UV-C range, such as aromatics (X. Wang et al., 2024). We do not expect this interference to be significant during CarCavAQS as none of the high O_3 days were influenced by smoke (Pollack et al., 2023), and concentrations of all measured aromatics were relatively low (mean: 0.29 ppbv; max: 5.2 ppbv). Additional trace gas instruments whose data are used in this work include a Thermo 48C non-dispersive infrared absorption analyzer for carbon monoxide (CO), a Picarro G2508 cavity ring-down spectrometer for CH_4 , and an Eco Physics CLD 780 TR chemiluminescence NO detector outfitted with custom inlets for NO_x and total oxidized reactive nitrogen (NO_y). NO_2 and NO_y were reduced to NO by a UV (395 nm) photolytic converter and a heated (320°C) molybdenum converter, respectively, both positioned at the inlet tip (Pollack et al., 2023). Gaseous nitric acid (HNO_3) was collected in 24-hr intervals (midnight to midnight) using University Research Glassware (URG) annular denuder samplers and quantified offline by ion chromatography (Naimie et al., 2022). The National Park Service routinely monitors O_3 and standard meteorological parameters (temperature, pressure, relative humidity, solar radiation, wind speed and direction) at CAVE; the rest of the instruments were only deployed during CarCavAQS.

Results presented in this study build on a source attribution of the CarCavAQS non-methane VOC data set determined using the EPA Positive Matrix Factorization (PMF) v5.0 model. Details on the PMF methodology and solution are provided by Pan et al. (2023). The PMF results serve two roles in this current study: to describe the variability of VOC sources over the study period and to inform model scenarios with targeted reductions/increases of VOCs from specific source categories.

2.2. Modeling Approach

The Framework for 0-D Atmospheric Modeling (F0AM v4.2.2; Wolfe et al., 2016) was used to evaluate the sensitivity of O_3 production to changes in precursor concentrations. Simulations were initialized with and constrained to observed NO_x , CO, CH_4 , and primary VOCs, as well as meteorological inputs (temperature, pressure, and relative humidity). While the representation of physical processes like dilution, deposition, and entrainment is highly simplified in 0-D “box” models, they serve as valuable tools for sensitivity analyses if simulated levels of unconstrained secondary species such as O_3 are in reasonable agreement with observations. Such agreement indicates that the model appropriately represents the photochemical processes active in oxidant production (Souri et al., 2023).

Box models can reasonably capture observed O_3 concentrations when a large fraction of O_3 at a given site is produced by in situ chemistry (Edwards et al., 2013, 2014; McDuffie et al., 2016; Ninneman & Jaffe, 2021; Xiong et al., 2023). O_3 in photochemically aged air masses depleted of NO_x and primary VOCs is likely to be underestimated by a box model, as substantial O_3 production occurs upwind of the location of interest (Xue et al., 2013). In this study, O_3 sensitivity results are primarily based on CarCavaQS days when photochemically fresh air masses impacted CAVE. Photochemical age was assessed with the NO_x/NO_y ratio, where days with maximum 1-hr $NO_x/NO_y > 0.8$ were considered influenced by photochemically fresh air masses (Kleinman et al., 2008; Warneke et al., 2007). The ratio calculation was restricted to the morning hours (06:00–10:00 LT) to capture the characteristics of air masses affecting CAVE before substantial planetary boundary layer (PBL) expansion and photochemical processing occurred. Based on this threshold, 11 days of CarCavaQS were selected for detailed O_3 sensitivity analysis. Other characteristics that distinguish these days from the rest of the campaign are discussed in Section 3.1. Limited model analysis is conducted for a set of high O_3 days influenced by more aged emissions (Section 3.4).

A subset of the Master Chemical Mechanism (MCM v3.3.1; Jenkin et al., 2015) was used for the model chemistry scheme, containing near-explicit gas-phase degradation schemes for CH_4 and 27 primary VOCs, as well as relevant inorganic reactions, yielding a total of 2572 species and 7523 reactions. Data reduction criteria used by Pan et al. (2023) were applied to all VOC observations such that species with long periods of missing data and/or signal-to-noise ratios < 0.5 were excluded from the model constraints. Species not included in the MCM were “lumped” with other species that have similar reaction rate coefficients with the hydroxyl radical (OH; Table S2 in Supporting Information S1). The observational constraint on NO_x was partitioned by the model into NO and NO_2 at each time step assuming photostationary state. Photolysis rates were calculated using lookup tables from the NCAR Tropospheric Ultraviolet and Visible (TUV) radiation model (available at <https://www2.acom.ucar.edu/modeling/tuv-download>). To account for deviations from clear-sky conditions, a correction factor scaled by in situ pyranometer observations of solar radiation was applied to all calculated photolysis rates. Physical loss by dilution during PBL growth was simulated by applying a first-order loss rate (k_{dil} ; $5 \times 10^{-5} s^{-1}$, corresponding to a dilution lifetime of ~ 6 hr) to all model-calculated species. O_3 and other measured secondary species (OVOCs, PANs, $RONO_2$) were initialized at the first model time step but not further constrained.

Each simulation was initialized at midnight and integrated forward for 48 hr. Following the approach of Mayhew et al. (2022), daily observational constraints were duplicated to provide a 48-hr constraint of two repeated periods: the first 24-hr period was included for model spin-up and the second 24-hr period was considered as the model output. Further simulations showed that modeled O_3 mixing ratios were not affected when using a spin-up period longer than 24 hr. The model integration time step was set to 10 min and the model output was averaged to 1 hr for comparison with observations. Additional information on model setup is provided in Text S1 of the Supporting Information S1.

The model demonstrated considerable skill in capturing the observed variability in O_3 ($R^2 = 0.78$; Figure S3 in Supporting Information S1) and other unconstrained species (median R^2 for 16 unconstrained species = 0.60; Figure S4 in Supporting Information S1) during photochemically fresh days. An extended evaluation of model performance is provided in Text S2 of the Supporting Information S1. Sensitivity tests showed that among select parameters, modeled O_3 was most sensitive to changes in photolysis rates (Table S3 in Supporting Information S1). While direct measurements of photolysis rates were unavailable, we are confident in our approach of scaling TUV clear-sky calculations given the strong model-observation agreement for NO ($R^2 = 0.79$) and NO_2 ($R^2 = 0.90$).

The O_3 production rate ($P(O_3)$) was calculated from F0AM output as the net rate of O_x ($=O_3 + NO_2$) production:

$$\begin{aligned} P(O_3) = & k_{HO_2+NO}[HO_2][NO] + \sum k_{RO_2i+NO}[RO_2i][NO] \\ & - k_{OH+NO_2+M}[OH][NO_2][M] - P(RO_2NO_2) - P(RO_2NO_2) \\ & - k_{OH+O_3}[OH][O_3] - k_{HO_2+O_3}[HO_2][O_3] \\ & - k_{O(^1D)+H_2O}[O(^1D)][H_2O] - L(\text{alkenes} + O_3), \end{aligned} \quad (1)$$

where k terms are the rate coefficients and RO_2 are individual organic peroxy radicals. The negative terms in Equation 1 represent O_x loss pathways: the reaction between OH and NO_2 to form HNO_3 , the net production of organic nitrates (RONO_2 and RO_2NO_2), the reactions of OH and HO_2 with O_3 , the photolysis of O_3 followed by reaction of $\text{O}(^1\text{D})$ with water, and alkene ozonolysis reactions.

2.3. HYSPLIT Back-Trajectories

To examine air mass transport patterns influencing CAVE, back-trajectories were calculated using the NOAA Hybrid Single-Particle Lagrangian Integrated Trajectory model (HYSPLIT; Stein et al., 2015). We used meteorological reanalysis fields from the North American Mesoscale Forecast System (NAM-12), which have a 12 km horizontal resolution and a 3-hr temporal resolution (NCEI, 2023). Trajectories were initiated from CAVE at 100 m above model ground level and integrated backward for 48 hr, with a new trajectory initiated every 2 hr for the duration of CarCavAQS.

3. Results and Discussion

3.1. Variability in O_3 and Its Precursors During CarCavAQS

Observations at CAVE during summer 2019 revealed significant day-to-day variability in O_3 and its precursors. While at least 6 days with MDA8 $\text{O}_3 > 70$ ppbv occurred in 2019 (O_3 measurements in 2019 began on 7/18; Pollack et al., 2023), only 2 fell within the period when VOC measurements were available (7/30–9/2). Hourly O_3 surpassed 70 ppbv on 7 days during this period, although those days did not always align with elevated NO_x and VOCs (Figure 2). We address this variability by separating the 35 days with VOC measurements into three distinct groups: photochemically fresh/O&G-influenced (abbreviated as fresh/O&G), photochemically aged/O&G-influenced (aged/O&G), and photochemically aged/background (aged/bkg). The criteria used to determine these groups are listed in Table 1. As discussed in Section 2.2, the NO_x/NO_y ratio was used to infer photochemical age, and 11 days with maximum morning $\text{NO}_x/\text{NO}_y > 0.8$ were deemed appropriate for O_3 sensitivity analysis with FOAM. These 11 days fall into the fresh/O&G group and represent days when emissions in the surrounding region (including the Permian basin) account for a large portion of photochemical O_3 production. Modeled O_3 concentrations for the 11 fresh/O&G days are included in Figure 2e. Days with lower NO_x/NO_y (aged/O&G and aged/bkg groups) represent periods of longer-range transport of O_3 and its precursors from upwind emission sources.

Aged/bkg days were further distinguished from fresh/O&G and aged/O&G days based on influence from different emission sources, as indicated by the *i*-*n*-pentane ratio. The *i*-*n*-pentane ratio is a robust indicator for identifying O&G influence, with ratios < 1 usually associated with O&G influence while ratios of 2 or more associated with traffic or other fossil fuel combustion sources (Gilman et al., 2013; Swarthout et al., 2013). Both pentane isomers were tightly correlated across the campaign ($R^2 = 0.99$), with a median ratio of 0.88, indicating persistent O&G influence. However, some variability in *i*-*n*-pentane was observed at low total VOC mixing ratios. Three days (categorized into the aged/bkg group) had a median *i*-*n*-pentane > 1 , reflecting background (non-O&G) emissions sources. Aged/bkg days were also characterized by the lack of a clear morning rise in O_3 (Figure 3a) and a less pronounced morning-to-afternoon decline in NO_x/NO_y (Figure 3b), indicating less active photochemistry than during fresh/O&G and aged/O&G days.

Distinct diurnal wind direction patterns were observed among the three groups of days (Figure 3c). Fresh/O&G days were characterized by primarily southerly/southeasterly winds (the direction of the Permian basin). In contrast, aged/O&G days exhibited a shift in wind direction from westerly/northwesterly in the morning to southeasterly in the afternoon. Aged/bkg days consistently experienced westerly/northwesterly winds throughout the entire day. Wind speeds during aged/bkg days were slightly higher (mean ± 1 standard deviation: $4.3 \pm 1.9 \text{ m s}^{-1}$) than both fresh/O&G ($3.1 \pm 1.3 \text{ m s}^{-1}$) and aged/O&G ($3.6 \pm 2.3 \text{ m s}^{-1}$) days (campaign-wide mean: $3.5 \pm 2.0 \text{ m s}^{-1}$). The observed wind direction patterns indicate variable source influences, although in situ wind measurements at CAVE are potentially impacted by local terrain effects (Pan et al., 2023). HYSPLIT back-trajectories (Section 2.3) provide additional insight into regional transport patterns. Air masses during fresh/O&G days were primarily transported from the south/southeast (Figure 4a), directly over the Permian basin. During aged/O&G days, trajectories displayed more variability but still with substantial transport over the Permian (Figure 4b). In contrast, aged/bkg days were characterized by exclusively westerly/northwesterly transport and greatly reduced O&G influence (Figure 4c). We note that in the case of fresh/O&G days and especially aged/O&G

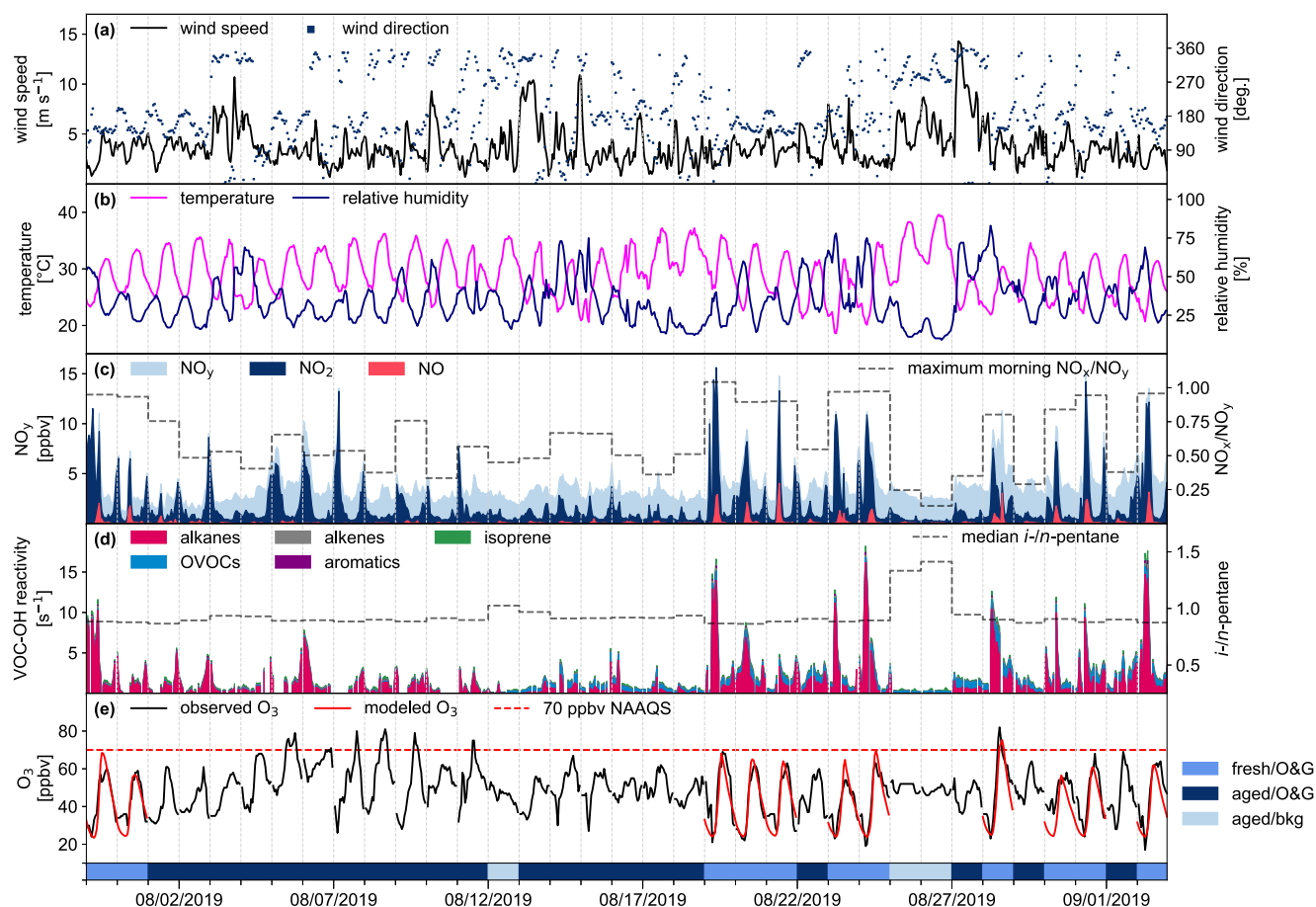


Figure 2. Time series of select meteorological and chemical parameters observed during CarCavAQS: (a) wind speed and direction; (b) temperature and relative humidity; (c) NO_y , NO_2 , NO , and the maximum morning (06:00–10:00 LT) NO_x/NO_y ratio; (d) the contributions of measured VOCs to VOC-OH reactivity (grouped by VOC type; Table S1 in Supporting Information S1) and the daily median i/n -pentane ratio; (e) 1-hr O_3 concentrations. The 70 ppbv NAAQS is shown for reference. The colored bars at the bottom panel show which days are grouped together based on photochemical age and emission influence (see text). Panel (e) includes modeled 1-hr O_3 concentrations for the 11 fresh/O&G days.

days, occasional longer-range transport patterns suggest a possible influence from more distant emission sources beyond the Permian basin. The abundance of alkanes and low i/n -pentane during both of these groups of days (Figure 2d) prompts us to consider other O&G basins, including the Eagle Ford and Barnett shale formations in Texas and the Anadarko basin in Oklahoma, as more likely dominant VOC sources rather than distant urban areas.

Figure 5 highlights several key differences among the three groups of days in terms of their 24-hr mean NO_y and VOC-OH reactivity budgets. It is clear that the observed variability is directly influenced by the differences in photochemical age and emission sources discussed above. NO_x accounted for 58%, 38%, and 20% of 24-hr mean NO_y for fresh/O&G, aged/O&G, and aged/bkg days, respectively. Mean ratios of PAN to HNO_3 , two NO_x

Table 1
Criteria Used to Categorize the 35 CarCavAQS Days Based on Photochemical Age and Emission Influence

Group	Number of days	Maximum morning NO_x/NO_y	Median i/n -pentane	Maximum daily 1-hr O_3 (ppbv)	Maximum daily 8-hr O_3 (ppbv)
Photochemically fresh/O&G-influenced (fresh/O&G)	11	>0.8	<1	64 ± 7	59 ± 5
Photochemically aged/O&G-influenced (aged/O&G)	21	<0.8	<1	66 ± 9	60 ± 7
Photochemically aged/background (aged/bkg)	3	<0.8	>1	53 ± 1	50 ± 2

Note. Observed mean ± 1 standard deviation of maximum daily 1- and 8-hr (MDA8) O_3 concentrations are included for each group.

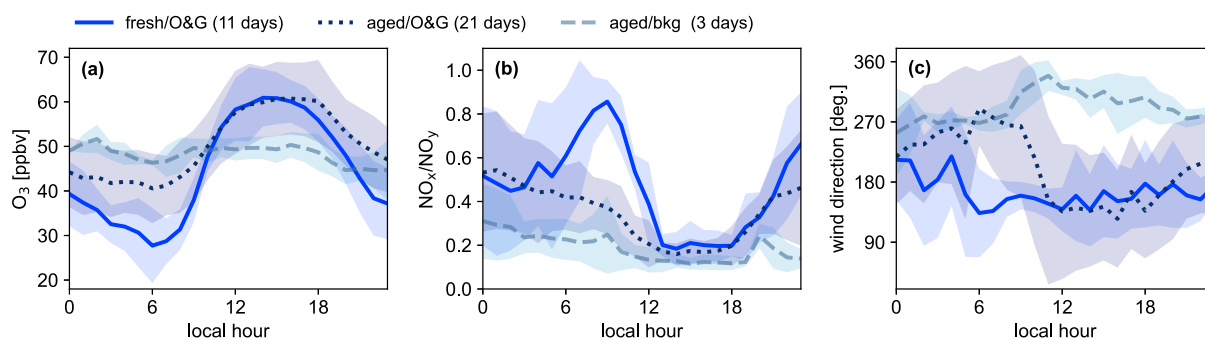


Figure 3. Comparison of diurnal variations in observed (a) O_3 , (b) NO_x/NO_y , and (c) wind direction across the three groups of CarCavAQs days. The lines and shading represent hourly composite means and standard deviations, respectively.

oxidation products, were similar for the fresh/O&G (0.54) and aged/O&G days (0.50), but much lower for the aged/bkg days (0.18). While PAN is efficiently produced from the oxidation of O&G-related VOCs, its lifetime at temperatures observed during CarCavAQs was limited to ~ 1 hr (Pollack et al., 2023). Lower PAN/ HNO_3 on aged/bkg days further emphasizes the lack of influence from fresh photochemistry. Additionally, the fraction of NO_y not accounted for by individually measured NO_y species (labeled “remaining NO_z ” in Figure 5, where $NO_z = NO_y - NO_x$) was largest in the aged/bkg group and smallest in the fresh/O&G group. This gap in the NO_y budget aligns with earlier study findings and is often attributed to organic nitrates and particulate nitrate species not measured individually (Day et al., 2003; Fahey et al., 1986). Regardless of the exact composition, these species are expected to form more as the photochemistry proceeds over time (Bertman et al., 1995; Zare et al., 2018).

The PMF analysis of CarCavAQs non-methane VOC observations presented by Pan et al. (2023) provides insight into the variability of VOC sources impacting CAVE during the study period. Of the seven source factors identified, three were associated with primary O&G emissions: Factor 1 was composed mainly of longer-lived alkanes (C_2 – C_7), Factor 2 was composed mainly of shorter-lived alkanes (C_7 – C_8), and Factor 3 included C_8 – C_{10} alkanes, ethylbenzene, and xylenes potentially tied to O&G pre-production processes. On average, Factors 1–3 accounted for the majority of the total VOC mixing ratio, showed strong correlations with NO_x and CH_4 , and were predominantly associated with the southeast wind sector (Pan et al., 2023; Pollack et al., 2023). Of the remaining four factors, two were characterized by OVOCs and $RONO_2$ associated with secondary chemical production (Factors 4 and 5), one included C_2 – C_4 alkenes attributed to a mixture of possible combustion sources (Factor 6), and the other was a regional background factor containing halocarbons, acetonitrile, and isoprene (Factor 7). To estimate the relative importance of each factor as a source of O_3 precursors, the factor contributions were compared among the groups of days in terms of their VOC-OH reactivity (Figures 5b and 5d), calculated as:

$$\text{VOC-OH reactivity} = k_{OH+X}[X], \quad (2)$$

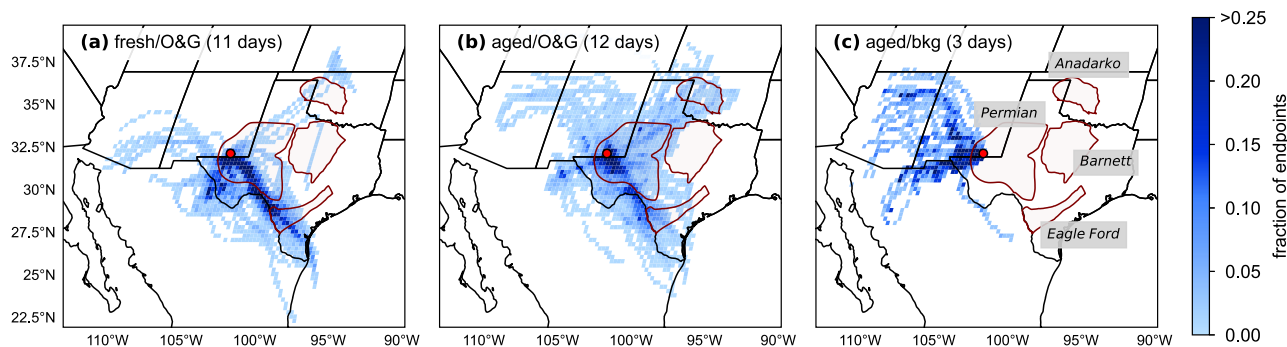


Figure 4. Comparison of 48-hr HYSPLIT back-trajectories across the three groups of CarCavAQs days. A total of 12 trajectories were initiated from CAVE for each day, with a new trajectory initiated every 2 hr. The color bar indicates the number of trajectory endpoints within a $0.25^\circ \times 0.25^\circ$ grid cell divided by the total number of trajectories for each group. The red dot shows the location of CAVE and the maroon polygons outline key O&G basins in the region (US EIA, 2016).

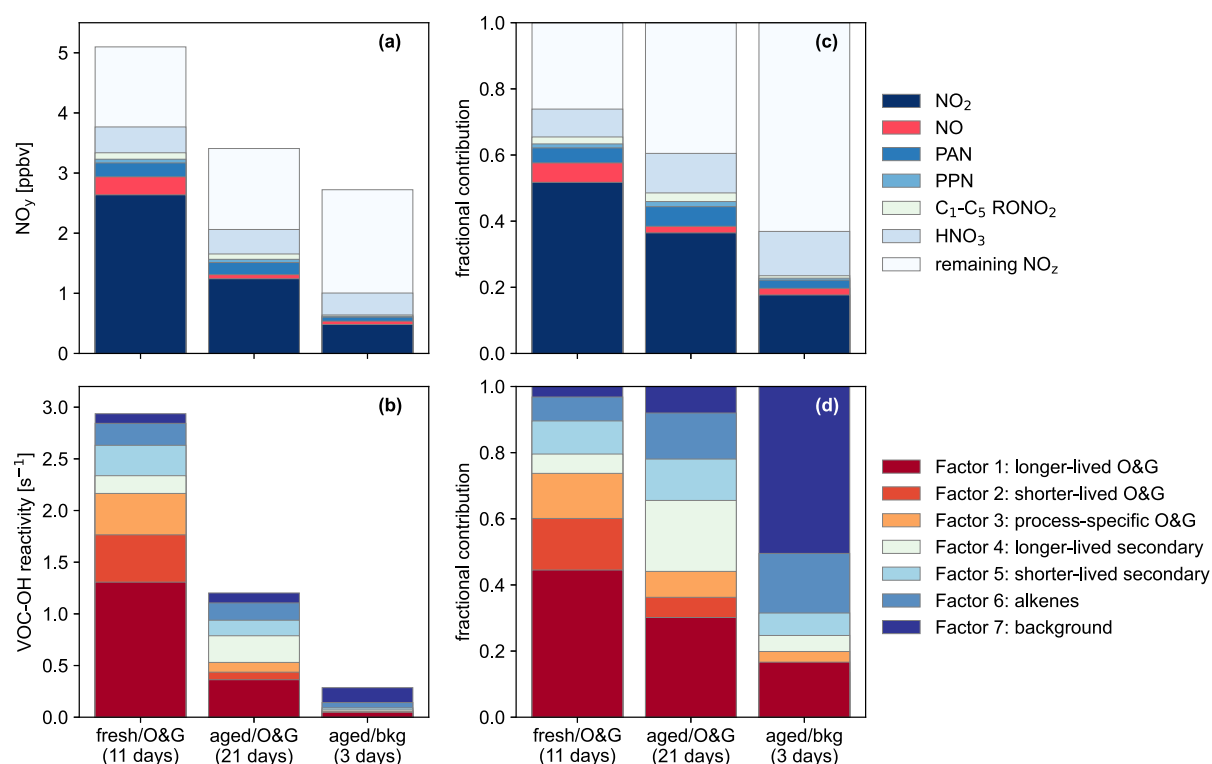


Figure 5. Comparison of 24-hr mean budgets of (a) observed NO_y compounds and (b) contributions of PMF factors to calculated VOC-OH reactivity across the three groups of CarCavaQS days. Panels (c) and (d) show normalized fractional contributions for NO_y and VOC-OH reactivity, respectively.

where $k_{\text{OH}+\text{X}}$ is the rate coefficient of species X with OH at 298 K and [X] is the species concentration. Rate coefficients for VOC-OH reactivity calculations are listed in Table S1 of the Supporting Information S1. VOC-OH reactivity is a useful metric for assessing the potential of a given VOC (or group of VOCs) to contribute to O_3 production, since the oxidation of VOCs by OH is often the rate-limiting step in the O_3 formation cycle (Abeleira et al., 2017; Benedict et al., 2020; Gilman et al., 2013). Fresh/O&G days exhibited the largest contributions from the O&G factors (Factors 1–3) to the calculated VOC-OH reactivity budget. The two secondary factors (Factors 4 and 5) exhibited large contributions on aged/O&G days. Factor 7 (background) was the largest contributor to VOC-OH reactivity on aged/bkg days.

Only three measured OVOCs (acetone, MEK, and MVK) met the data reduction criteria for inclusion in the PMF analysis of Pan et al. (2023), and therefore the contribution of Factors 4 and 5 should be considered as a lower limit of the true contribution of secondary species to total VOC-OH reactivity. Acetaldehyde (measured by the PTR-MS but not part of the PMF), together with HCHO, propionaldehyde, butyraldehyde, hexaldehyde, and benzaldehyde (measured with DNPH cartridges) contributed approximately 1.4, 1.6, and 0.7 s^{-1} of additional 24-hr mean VOC-OH reactivity to fresh/O&G, aged/O&G, and aged/bkg days, respectively (Figure S5 in Supporting Information S1). Details on how these contributions were estimated are provided in Text S3 of the Supporting Information S1. Other OVOCs that likely add to VOC-OH reactivity include alcohols, which were not measured in this study but may have both primary and secondary sources in O&G regions (Koss et al., 2015).

The following 2 sections discuss O_3 production sensitivity on fresh/O&G days. High O_3 days part of the aged/O&G group are examined in Section 3.4. Given the apparent lack of in situ O_3 production, aged/bkg days will not be a focus of this paper.

3.2. O_3 Production Sensitivity on Photochemically Fresh Days

A useful feature of box models is their ability to track radical production and loss rates, which offers insight into the sensitivity of O_3 production to NO_x and VOC precursors. Figure 6 shows the mean model-calculated primary radical production ($P(\text{RO}_x)$) and loss ($L(\text{RO}_x)$) budgets for the 11 fresh/O&G days, where

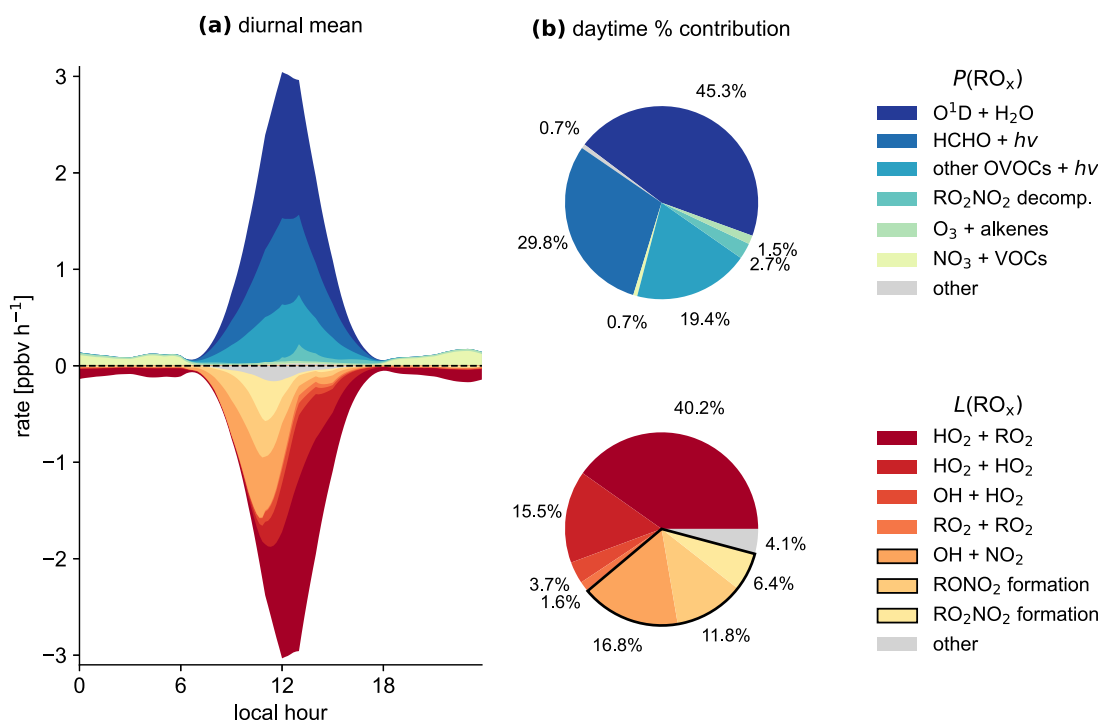


Figure 6. (a) Model-calculated mean diurnal profile of primary radical production ($P(\text{RO}_x)$) and loss ($L(\text{RO}_x)$) pathways for the 11 fresh/O&G days. (b) Daytime (06:00–18:00 LT) percent contribution of each RO_x production/loss pathway. Radical- NO_x termination reactions are outlined in black.

$\text{RO}_x = \text{OH} + \text{HO}_2 + \text{RO}_2$. The photolysis of OVOCs was the dominant primary radical source, accounting for 49.2% of daytime $P(\text{RO}_x)$, followed closely by the photolysis of O_3 and the subsequent reaction of O^1D with H_2O (45.3%). HCHO stood out as the main contributor out of all photolabile OVOCs, accounting for 29.8% of daytime $P(\text{RO}_x)$. Other OVOCs with significant contributions included methylglyoxal, acetaldehyde, and MEK. These OVOCs are efficiently produced from O&G-related primary VOCs such as alkanes and aromatics, and have been recognized as important primary radical sources in other O&G regions (Chen et al., 2020, 2022; Edwards et al., 2014). The model-calculated O_3 production rate ($P(\text{O}_3)$; Equation 1) peaked at approximately noon each day, with daily maximum values ranging from 10 to 18 ppbv h^{-1} (Figure S6 in Supporting Information S1). These rates are similar to prior measurements of $P(\text{O}_3)$ in the northern Colorado Front Range ($\sim 14 \text{ ppbv h}^{-1}$; Baier et al., 2017), but lower than those measured during high O_3 episodes in Houston, Texas ($\sim 40 \text{ ppbv h}^{-1}$; Cazorla et al., 2012; Mao et al., 2010).

The chemical transition point between NO_x - and VOC-sensitive O_3 production depends on whether radical-radical reactions or radical- NO_x reactions dominate radical loss (Kleinman, 2005). The radical budget presented in Figure 6 indicates that morning versus afternoon photochemistry at CAVE was markedly different, with the majority (76%) of $L(\text{RO}_x)$ between 06:00 and 10:00 LT occurring through radical- NO_x reactions, as opposed to only 11% between 12:00 and 18:00 LT. Radical- NO_x termination reactions include the reaction between OH and NO_2 to form HNO_3 , as well as the net formation of organic nitrates (RONO_2 and RO_2NO_2). Radical-radical termination reactions, which dominate $L(\text{RO}_x)$ in the afternoon, include the combination of HO_2 and RO_2 , the HO_2 self-reaction, the combination of OH and HO_2 , and RO_2 self- or cross-reactions. Recent studies have also considered the uptake of HO_2 onto aerosol surfaces as an additional radical sink (Ivatt et al., 2022). While our simulations do not include heterogeneous processes, they are unlikely to affect our conclusions regarding O_3 production at CAVE. The maximum 24-hr $\text{PM}_{2.5}$ concentration during CarCavAQS was $13 \mu\text{g m}^{-3}$ (Naimie et al., 2022); significantly lower than in previous studies where aerosol HO_2 uptake was shown to have an impact on O_3 sensitivity (Dyson et al., 2023; Song et al., 2022).

The diurnal profile of $L(\text{RO}_x)$ (Figure 6a) suggests that O_3 production transitions from a VOC-sensitive regime in the morning to a NO_x -sensitive regime in the afternoon. Between 06:00 and 10:00 LT, as the radical pool begins to grow, the observed mean NO_x concentration was $6.7 \pm 4 \text{ ppbv}$ —enough to impose VOC-sensitivity on O_3

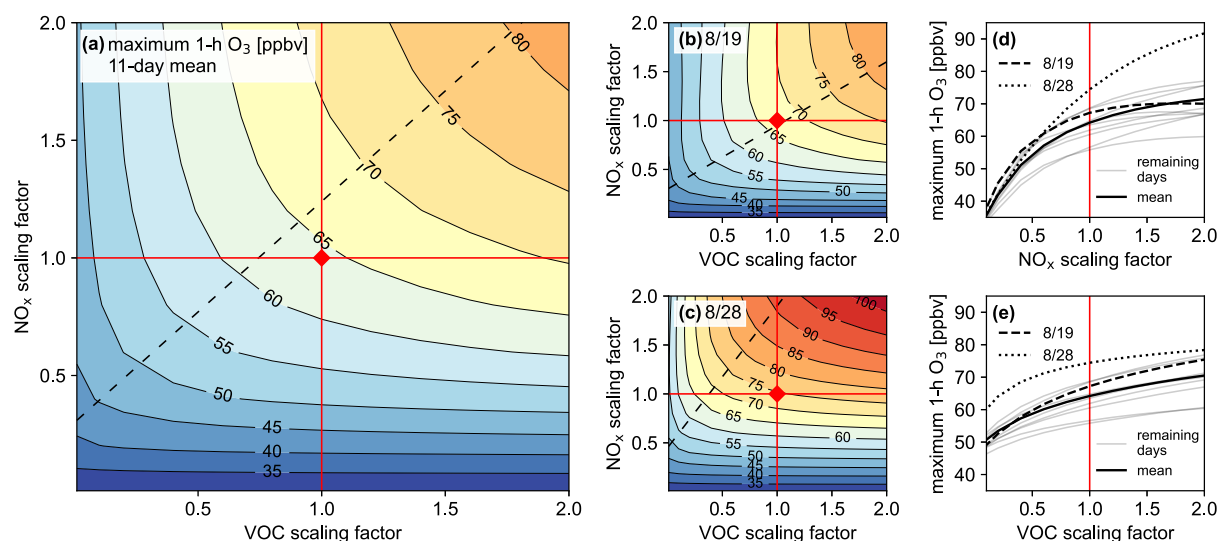


Figure 7. (a) Maximum 1-hr O₃ isopleths (mean of 11 fresh/O&G days) derived by scaling NO_x and primary VOC constraints by factors ranging from 0.01 to 2.0. Panels (b) and (c) show maximum 1-hr O₃ isopleths for individual days 8/19 and 8/28/2019, respectively. The dashed lines indicate the approximate O₃ “ridgeline” (i.e., the transition between NO_x- and VOC-sensitive regimes). Panels (d) and (e) show the modeled maximum 1-hr O₃ as a function of NO_x and VOC scaling factors, respectively. The diamond symbol in the center of panels (a)–(c) represents the model maximum O₃ at observed NO_x and VOC levels (scaling factor = 1.0). Red lines at scaling factors of 1.0 are included in each panel for reference.

formation by reacting with the majority of available radicals. By local noon (when $P(\text{RO}_x)$ was at its peak), NO_x rapidly declined to sub-ppbv levels, allowing radical-radical reactions to dominate $L(\text{RO}_x)$. O₃ production during the remaining daylight hours proceeded in a NO_x-sensitive regime. This regime shift aligns with about a twofold increase in the observed VOC/NO_x ratio from 96 ± 40 ppbC ppbv^{−1} in the morning to 194 ± 97 ppbC ppbv^{−1} in the afternoon. Similar sub-daily variations in O₃ production sensitivity have been reported at various sites impacted by large NO_x emissions (Mao et al., 2010; Rickly et al., 2023; Sakamoto et al., 2019; Sillman & West, 2009).

To visualize how O₃ responds to changing NO_x and VOCs, maximum O₃ isopleth diagrams were constructed for each of the 11 fresh/O&G days (Figure 7). This was done by running simulations across a 12×12 matrix of independently scaled NO_x and primary VOC constraints. All 27 primary VOCs were treated as a whole and subject to uniform scaling factors. The average isopleth diagram for the 11 fresh/O&G days (Figure 7a) reveals that maximum O₃ at observed precursor levels (i.e., at NO_x and VOC scaling factors of 1.0) was responsive to changes in both NO_x and VOCs, with a stronger sensitivity to NO_x. By comparing the slopes of the mean lines in Figures 7d and 7e, which show maximum O₃ as a function of NO_x and VOC scaling factors, respectively, we estimate that sensitivity to NO_x was approximately 1.5 times stronger than to VOCs. The prevalence of NO_x-sensitive conditions can also be inferred from the pie charts in Figure 6b, where radical-NO_x termination reactions accounted for less than half (35%) of total $L(\text{RO}_x)$ during daytime (06:00–18:00 LT).

The isopleths plotted in Figure 7a represent an average of the 11 fresh/O&G days, and individual days varied as to where O₃ production at observed precursor levels laid relative to the regime transition point (i.e., the O₃ “ridgeline” on the isopleth diagram). Isopleths for each day are shown in Figure S7 of the Supporting Information S1, and two examples with notably different sensitivity are included in panels (b) and (c) of Figure 7. On 8/19, maximum O₃ at observed precursor levels showed 1.1 times greater sensitivity to VOCs than to NO_x, while on 8/28, maximum O₃ showed 4.4 times greater sensitivity to NO_x than to VOCs. The observed VOC/NO_x ratio in the morning of 8/28 (154 ± 35 ppbC ppbv^{−1}) was much higher compared to 8/19 (95 ± 20 ppbC ppbv^{−1}). Other characteristics that may have influenced the varying O₃ production sensitivities on these days are discussed in Text S4 of the Supporting Information S1.

On average, our results indicate that NO_x emission reductions would be the most effective strategy for reducing maximum O₃ at CAVE. However, given the proximity of O₃ production to the regime transition point, VOC emission reductions can also be important, especially when CAVE is impacted by air masses with lower VOC/NO_x. Concurrent reduction of both NO_x and VOC emissions would also lead to reduced HCHO production, which is important to consider in the context of O₃ given HCHO's key role as a primary radical source. A recent

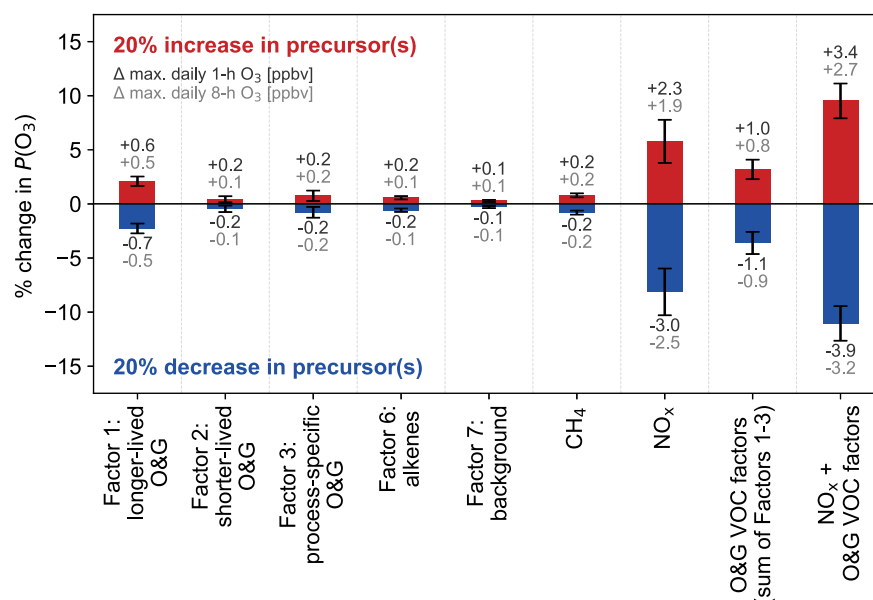


Figure 8. Modeled changes in the daytime (06:00–18:00 LT) mean O_3 production rate ($P(O_3)$) based on a $\pm 20\%$ change in precursor constraints. The bars show the mean sensitivity results for the 11 fresh/O&G days, with error bars representing ± 1 standard deviation. Absolute changes in modeled maximum daily 1- and 8-hr O_3 mixing ratios (mean of 11 fresh/O&G days) are included for additional context.

study concluded that over 90% of HCHO over the Permian basin results from secondary formation, and the yield of HCHO is as sensitive to NO_x emissions as it is to VOC emissions (Dix et al., 2023).

3.3. Precursor-Specific Impacts on O_3

A series of simulations were performed to examine how specific precursors impact O_3 production at CAVE. The constraint on a select precursor (or group of precursors) was independently varied by $\pm 20\%$, and the resulting daytime mean O_3 production rate ($P(O_3)$; Equation 1) was compared to the base case simulation. Figure 8 displays the mean sensitivity results for the 11 fresh/O&G days, and individual day's results are shown in Figure S9 of the Supporting Information S1. To keep this analysis relevant to realistic emission control scenarios, VOC constraints were adjusted in groups based on the PMF source factors described in Pan et al. (2023), while unapportioned VOCs not part of the PMF solution were left unscaled. The PMF-reconstructed concentrations accounted for >95% of the total observed VOC mixing ratio across the 11 fresh/O&G days. PMF Factors 4 (longer-lived secondary) and 5 (shorter-lived secondary) were not included in the sensitivity analysis because these factors mainly consisted of secondary species (OVOCs and $RONO_2$) that were left unconstrained in the model. To show how simulated changes in $P(O_3)$ translate to changes in O_3 concentrations during the fresh/O&G days, absolute changes in modeled maximum daily 1- and 8-hr (MDA8) O_3 are also included in Figure 8. We note that relative changes were applied to precursor constraints, which in the base case simulation are equal to observed mixing ratios. This sensitivity analysis therefore reflects the response of in situ O_3 production to changes in NO_x or VOC mixing ratios rather than changes in emissions. Such results are still useful as qualitative indicators of how different emission control strategies impact O_3 (Cardelino & Chameides, 1995; Kleinman et al., 2000).

A $+20\%/ -20\%$ change in the NO_x constraint impacted daytime mean $P(O_3)$ by $5.8\%/ -8.1\%$, surpassing the effect of changing any individual PMF VOC factor and the aggregated O&G VOC factors (sum of Factors 1–3) by the same relative amount. This result is consistent with the earlier conclusion that O_3 production at CAVE is more NO_x -sensitive. Out of the individual PMF factors, $\pm 20\%$ changes in Factor 1 (longer-lived O&G) had the largest effect on O_3 , followed by Factor 3 (process-specific O&G), Factor 6 (alkenes), Factor 2 (shorter-lived O&G), and Factor 7 (background). It is worth noting that the compounds included in Factor 1 (primarily C_2 – C_7 alkanes) had larger impacts on O_3 than other VOC groups due to their high abundance (mean concentrations of ethane and propane during fresh/O&G days were 28 and 25 ppbv, respectively). Alkenes and other more reactive VOCs were present at much lower concentrations (0.31 and 0.06 ppbv for ethene and propene, respectively). CH_4 , with a

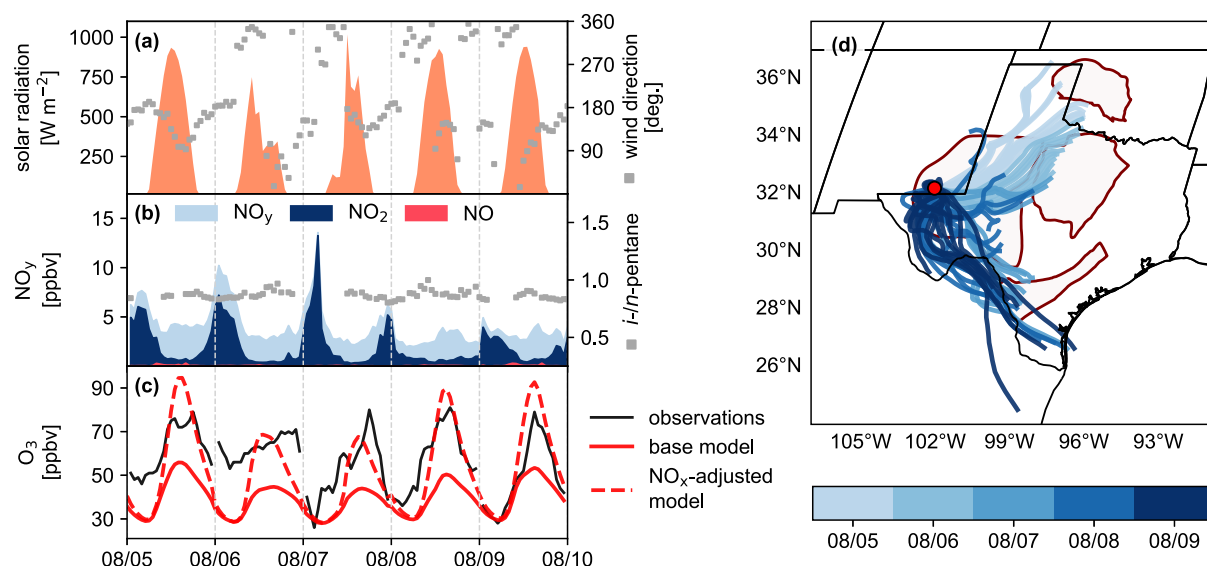


Figure 9. Time series of (a) solar radiation (left axis) and wind direction (right axis), (b) NO_y , NO_2 , NO (left axis) and i/n -pentane ratios (right axis), and (c) O_3 concentrations during 5 consecutive high O_3 observed at CAVE. Also shown in (c) are modeled O_3 concentrations under the base case conditions (see text), and under a second model scenario in which the model NO_x was adjusted to match observed NO_y . Panel (d) shows 48-hr HYSPLIT back-trajectories initiated from CAVE every 2 hr during the 5 days. The red dot represents the location of CAVE, and the maroon polygons outline major O&G basins in the region. See Figure 1 for O&G basin labels.

mean concentration of 2.13 ppmv, had a relatively minor impact on local O_3 production due to its significantly lower reactivity compared to higher molecular weight VOCs. While the sensitivity results for precursor increases/decreases were largely symmetric, a 20% increase in precursor(s) tended to yield a slightly smaller change than a 20% decrease, especially for NO_x . This pattern is also evident in Figure 7, where reducing the NO_x scaling factors from 1.0 yields steeper changes in O_3 compared to increases above 1.0.

Figure 8 also includes sensitivity results for a $\pm 20\%$ change in the O&G VOC factors together with NO_x . Notably, for a 20% decrease, the cumulative impact of O&G VOC factors and NO_x on $P(\text{O}_3)$ was approximately 1.4 times greater compared to a 20% decrease in NO_x alone. This suggests that while O_3 production at CAVE is generally NO_x -sensitive, both NO_x and VOC emission reductions would help lower O_3 . This mixed sensitivity is consistent with findings in various urban areas (Berezina et al., 2020; Jin & Holloway, 2015; Koplitz et al., 2022), as well as at a site near the Denver-Julesburg O&G basin in Colorado. Earlier box modeling studies conducted at the Boulder Atmospheric Observatory (BAO) showed that summertime O_3 production was primarily sensitive to NO_x but still responsive to changes in O&G-related VOCs (Lindaas et al., 2019; McDuffie et al., 2016). Targeting emissions from regional O&G activities should be a priority for reducing O_3 at CAVE since these activities are the dominant source of both NO_x and VOCs to the park (Pan et al., 2023; Pollack et al., 2023). This is supported by robust correlations between NO_x and the three O&G VOC factors, along with strong correlations between NO_x and individual O&G tracer species (C_1 - C_3 alkanes; Pollack et al., 2023). Additionally, both NO_x and O&G-related VOCs were primarily associated with the southeast wind sector, where there are no major cities within ~ 200 km. The absence of weekday-weekend differences in NO_x , which would typically indicate strong contributions from urban traffic sources, further suggests a lack of influence from urban NO_x (Pollack et al., 2023).

3.4. High O_3 on Photochemically Aged Days

Although the O_3 production sensitivity results discussed above are based on the 11 fresh/O&G days deemed appropriate for treatment with a box model, this excludes the highest O_3 days observed during CarCavaQS. In this section, we examine a 5-day episode (8/5–8/10/2019) during which 1-hr O_3 surpassed 70 ppbv on each day. Observed MDA8 O_3 was >70 ppbv on 8/5 and 8/8, and >65 ppbv on 8/6, 8/7, and 8/9. Based on NO_x/NO_y and i/n -pentane ratios (Section 3.1), these days were sorted into the aged/O&G group.

Figure 9 presents a time series of this 5-day episode. Despite variations in local wind direction, consistent i/n -pentane ratios <1 indicate that the air masses impacting CAVE during this episode were predominantly influenced by O&G emissions. FOAM simulations for these 5 days under the same configurations employed for the 11

fresh/O&G days (i.e., constrained to observed NO_x and primary VOCs, constant dilution rate, constant background O_3) substantially underestimate O_3 in comparison to observations (see base model O_3 in Figure 9c). Integrating the modeled $P(\text{O}_3)$ for the 5 days results in only 22 ± 9 ppbv of O_3 produced per day (compared to 53 ± 8 ppbv O_3 produced per day during fresh/O&G days), meaning that significant O_3 on these days must have formed during photochemical processing upwind. This is consistent with the markers of strong photochemical aging, including lower NO_x/NO_y ratios (NO_x accounted for 45% of 24-hr mean NO_y compared to 58% during fresh/O&G days) and enhanced secondary VOCs (longer- and shorter-lived secondary PMF factors contributed 22% and 14% to the 24-hr mean VOC-OH reactivity, respectively, in contrast to 6% and 10% during fresh/O&G days).

HYSPLIT back-trajectories show that air masses on each of the 5 days passed over the Permian basin before arrival at CAVE, with a gradual shift from northeasterly transport on 8/5 and 8/6 toward stronger southeasterly transport starting on 8/7 (Figure 9d). This suggests that, in addition to the Permian basin, air masses on 8/5 and 8/6 may have also been influenced by emissions from the more distant Anadarko and Barnett O&G production regions, while air masses on 8/7 onwards may have carried additional emissions from the Eagle Ford shale play. This aligns with the residence time analysis conducted by Pan et al. (2023), which showed that the longer-lived secondary PMF factor was associated with enhanced transport from more distant O&G regions.

Modeled radical loss rates indicate that in situ O_3 production during the 5-day high O_3 episode was strongly NO_x -sensitive, with only 9% of daytime radical loss occurring through reaction with NO_x (compared to 35% during fresh/O&G days). The tendency toward stronger NO_x sensitivity with photochemical age has been observed previously (see Sillman (1999) and references therein). A fraction of the transported O_3 may have formed under VOC-sensitive conditions when closer to NO_x sources, owing to the titration of O_3 by NO and efficient removal of radicals by NO_x . The timing of transition to NO_x -sensitive conditions depends on the rate of NO_x loss along the air mass trajectory (Sillman, 1999).

To test whether sufficient NO_x was present in the air mass to account for upwind O_3 production during transport to CAVE, we re-ran the F0AM simulations constraining the model NO_x with observed NO_y for this 5-day episode (see NO_x -adjusted model O_3 in Figure 9c). NO_y acts as an estimate of the amount of NO_x at the time of emission, assuming minimal depositional loss of HNO_3 or other NO_z compounds during transport. We note that this model scenario should be interpreted qualitatively since it does not account for the upwind photochemical oxidation of primary VOCs. Modeled O_3 in this scenario more closely reproduces the observed high O_3 , indicating that a large fraction of the observed O_3 was indeed formed during transport rather than in situ. We note that O_3 concentrations predicted by the box model depend on the chosen dilution rate and background O_3 level, which, given mixing effects, are not expected to be constant along the air mass trajectory. Discrepancies between observed and modeled O_3 in the NO_x -adjusted scenario, particularly in the early mornings of 8/5–8/8, may be caused by variations in background O_3 not captured by the model. A more comprehensive assessment of the photochemical evolution of air masses from the time of emission to arrival at CAVE would require a 3-D chemical transport model (CTM). However, future CTM studies will need to consider uncertainties and potential biases in O&G emissions depending on the chosen inventory (Ahmadov et al., 2015; Pétron et al., 2014).

4. Summary and Conclusions

We applied a 0-D photochemical box model (F0AM) to an extensive O_3 precursor data set collected at CAVE during summer 2019. Days during the study period were divided into three groups based on variations in photochemical age and emission influence: fresh/O&G, aged/O&G, and aged/bkg. Fresh/O&G days were characterized by high morning NO_x/NO_y ratios (>0.8), the predominant influence of O&G-related VOCs to VOC-OH reactivity, and consistent air mass back-trajectories indicating transport from the Permian basin. Aged/O&G days had lower NO_x/NO_y , a greater contribution of secondary VOCs to VOC-OH reactivity, and transport patterns that, while more variable, still indicated influence from O&G production regions. Aged/bkg days exhibited considerably less active photochemistry, with no clear diurnal patterns in O_3 or NO_x/NO_y , much lower total VOC levels, and persistent westerly/northwesterly transport—consistent with greatly reduced O&G influence. Our analysis primarily focuses on the 11 fresh/O&G days, which represent periods when most of the observed O_3 at CAVE can be attributed to in situ photochemical production.

An analysis of model-calculated radical loss rates suggests that O_3 production during the 11 fresh/O&G days was VOC-sensitive in the morning and NO_x -sensitive in the afternoon. Isopleth diagrams illustrate that maximum

daily O_3 was most responsive to NO_x , but close to the transition between NO_x - and VOC-sensitive regimes. In situ O_3 production is therefore subject to changing sensitivity with relatively small variations in the VOC/ NO_x ratio. Additional sensitivity analyses showed that reductions in both NO_x and O&G-related VOCs can help lower O_3 production, with NO_x reductions generally proving more effective.

Observed maximum daily O_3 was generally higher on aged/O&G days, including 2 days with MDA8 O_3 >70 ppbv. We examined a 5-day high O_3 episode (part of the aged/O&G group) during which air masses impacting CAVE were transported from upwind O&G production regions (Anadarko, Barnett, and Eagle Ford) in addition to the Permian basin. While the model could not reproduce the high O_3 episode when constrained to observed precursor levels, improved model-observation agreement was achieved by constraining NO_x in the model with observed NO_y . This confirms that a large portion of the O_3 on these days was not formed locally but instead during transport to CAVE. Given the mixed O_3 production sensitivity on fresh/O&G days, emissions of both NO_x and VOCs likely contributed to the initial accumulation of O_3 in the air masses impacting CAVE during aged/O&G days. These aged air masses were strongly NO_x -sensitive upon arrival at CAVE, suggesting that the extent of additional O_3 production after the air masses moved downwind of emission sources was determined by the quantity of emitted NO_x .

Reducing NO_x emissions from O&G activities might be efficiently realized through a targeted reduction of emissions from well drilling and completion activities, as indicated by a recent satellite-based analysis of NO_x emissions from the Permian basin during the COVID-19 pandemic. Reduced O&G demand in early 2020 led to a temporary decline in production and drilling activities, resulting in lower NO_x emissions particularly in areas with intensive drilling compared to areas with only production (Serrano-Calvo et al., 2023). A path for reducing emissions from drilling operations without removing those activities is the implementation of electrified, grid-powered drill rigs (Ericson et al., 2019; Ku et al., 2024). The findings related to O_3 production sensitivity presented in this study are expected to apply to other receptor sites in the broader west Texas/southeastern New Mexico region. This includes Guadalupe Mountains National Park (GUMO), another protected, federal Class 1 area ~50 km southwest of CAVE, where measured O_3 concentrations correlate closely with those at CAVE (Pollack et al., 2023).

Conflict of Interest

The authors declare no conflicts of interest relevant to this study.

Data Availability Statement

Data collected during CarCavAQS are archived at <https://doi.org/10.25675/10217/235481> (Sullivan et al., 2022). O_3 and meteorological data collected by the NPS are available for download from <https://ard-request.air-resource.com/> (NPS, 2024). FOAM v4.2.2 is available for download from <https://doi.org/10.5281/zenodo.6984581> (Wolfe et al., 2023).

Acknowledgments

This work is supported by the National Park Service (NPS) under Agreement Number P20AC00679 with Colorado State University. We thank Glenn Wolfe for his open-source FOAM model, the University of Leeds for the provision of the MCM v3.3.1, and the NOAA Air Resources Laboratory (ARL) for the provision of the HYSPLIT transport model. Additionally, we acknowledge Erin McDuffie and Jeffrey Pierce for their help with the model setup, Elena Cope for processing the PAN data, and the NPS staff at Carlsbad Caverns National Park for supporting the field study.

References

- Abeleira, A., Pollack, I. B., Sive, B., Zhou, Y., Fischer, E. V., & Farmer, D. K. (2017). Source characterization of volatile organic compounds in the Colorado Northern Front Range Metropolitan Area during spring and summer 2015. *Journal of Geophysical Research: Atmospheres*, 122(6), 3595–3613. <https://doi.org/10.1002/2016JD026227>
- Ahmadov, R., McKeen, S., Trainer, M., Banta, R., Brewer, A., Brown, S., et al. (2015). Understanding high wintertime ozone pollution events in an oil- and natural gas-producing region of the western US. *Atmospheric Chemistry and Physics*, 15(1), 411–429. <https://doi.org/10.5194/acp-15-411-2015>
- Allen, D. T. (2016). Emissions from oil and gas operations in the United States and their air quality implications. *Journal of the Air & Waste Management Association*, 66(6), 549–575. <https://doi.org/10.1080/10962247.2016.1171263>
- Baier, B., Brune, W., Miller, D., Blake, D., Long, R., Wisthaler, A., et al. (2017). Higher measured than modeled ozone production at increased NO_x levels in the Colorado Front Range. <https://doi.org/10.5194/acp-2016-1089>
- Barkley, Z., Davis, K., Miles, N., Richardson, S., Deng, A., Hmiel, B., et al. (2023). Quantification of oil and gas methane emissions in the Delaware and Marcellus basins using a network of continuous tower-based measurements. *Atmospheric Chemistry and Physics*, 23(11), 6127–6144. <https://doi.org/10.5194/acp-23-6127-2023>
- Benedict, K. B., Prenni, A. J., El-Sayed, M. M., Hecobian, A., Zhou, Y., Gebhart, K. A., et al. (2020). Volatile organic compounds and ozone at four national parks in the southwestern United States. *Atmospheric Environment*, 239, 117783. <https://doi.org/10.1016/j.atmosenv.2020.117783>
- Benedict, K. B., Zhou, Y., Sive, B. C., Prenni, A. J., Gebhart, K. A., Fischer, E. V., et al. (2019). Volatile organic compounds and ozone in Rocky Mountain National Park during FRAPPÉ. *Atmospheric Chemistry and Physics*, 19(1), 499–521. <https://doi.org/10.5194/acp-19-499-2019>

- Berezina, E., Moiseenko, K., Skorokhod, A., Pankratova, N. V., Belikov, I., Belousov, V., & Elansky, N. F. (2020). Impact of VOCs and NO_x on ozone formation in Moscow. *Atmosphere*, 11(11), 1262. <https://doi.org/10.3390/atmos11111262>
- Bernays, N., Jaffe, D. A., Petropavlovskikh, I., & Effertz, P. (2022). Comment on "Comparison of ozone measurement methods in biomass burning smoke: An evaluation under field and laboratory conditions" by Long et al. (2021). *Atmospheric Measurement Techniques*, 15(10), 3189–3192. <https://doi.org/10.5194/amt-15-3189-2022>
- Bertman, S. B., Roberts, J. M., Parrish, D. D., Buhr, M. P., Goldan, P. D., Kuster, W. C., et al. (1995). Evolution of alkyl nitrates with air mass age. *Journal of Geophysical Research*, 100(D11), 22805–22813. <https://doi.org/10.1029/95JD02030>
- Cardelino, C., & Chameides, W. (1995). An observation-based model for analyzing ozone precursor relationships in the urban atmosphere. *Journal of the Air & Waste Management Association*, 45(3), 161–180. <https://doi.org/10.1080/10473289.1995.10467356>
- Carter, W. P., & Seinfeld, J. H. (2012). Winter ozone formation and VOC incremental reactivities in the Upper Green River Basin of Wyoming. *Atmospheric Environment*, 50, 255–266. <https://doi.org/10.1016/j.atmosenv.2011.12.025>
- Cazorla, M., Brune, W. H., Ren, X., & Lefer, B. (2012). Direct measurement of ozone production rates in Houston in 2009 and comparison with two estimation methods. *Atmospheric Chemistry and Physics*, 12(2), 1203–1212. <https://doi.org/10.5194/acp-12-1203-2012>
- Chameides, W., & Walker, J. C. G. (1973). A photochemical theory of tropospheric ozone. *Journal of Geophysical Research*, 78(36), 8751–8760. <https://doi.org/10.1029/JC078i036p08751>
- Chen, T., Xue, L., Zheng, P., Zhang, Y., Liu, Y., Sun, J., et al. (2020). Volatile organic compounds and ozone air pollution in an oil production region in northern China. *Atmospheric Chemistry and Physics*, 20(11), 7069–7086. <https://doi.org/10.5194/acp-20-7069-2020>
- Chen, T., Zheng, P., Zhang, Y., Dong, C., Han, G., Li, H., et al. (2022). Characteristics and formation mechanisms of atmospheric carbonyls in an oilfield region of northern China. *Atmospheric Environment*, 274, 118958. <https://doi.org/10.1016/j.atmosenv.2022.118958>
- Coggon, M. M., Gkatzelis, G. I., McDonald, B. C., Gilman, J. B., Schwantes, R. H., Abuhassan, N., et al. (2021). Volatile chemical product emissions enhance ozone and modulate urban chemistry. *Proceedings of the National Academy of Sciences of the United States of America*, 118(32), e2026653118. <https://doi.org/10.1073/pnas.2026653118>
- Cohen, A. J., Brauer, M., Burnett, R., Anderson, H. R., Frostad, J., Estep, K., et al. (2017). Estimates and 25-year trends of the global burden of disease attributable to ambient air pollution: An analysis of data from the Global Burden of Diseases Study 2015. *The Lancet*, 389(10082), 1907–1918. [https://doi.org/10.1016/S0140-6736\(17\)30505-6](https://doi.org/10.1016/S0140-6736(17)30505-6)
- Crosman, E. (2021). Meteorological drivers of Permian Basin methane anomalies derived from TROPOMI. *Remote Sensing*, 13(5), 896. <https://doi.org/10.3390/rs13050896>
- Dalsøren, S. B., Myhre, G., Hodnebrog, i., Myhre, C. L., Stohl, A., Pisso, I., et al. (2018). Discrepancy between simulated and observed ethane and propane levels explained by underestimated fossil emissions. *Nature Geoscience*, 11(3), 178–184. <https://doi.org/10.1038/s41561-018-0073-0>
- Day, D. A., Dillon, M. B., Wooldridge, P. J., Thornton, J. A., Rosen, R. S., Wood, E. C., & Cohen, R. C. (2003). On alkyl nitrates, O₃, and the "missing NO_y". *Journal of Geophysical Research*, 108(D16), 4501. <https://doi.org/10.1029/2003JD003685>
- Dix, B., De Bruin, J., Roosenbrand, E., Vlemmix, T., Francoeur, C., Gorchov-Negron, A., et al. (2020). Nitrogen oxide emissions from U.S. oil and gas production: Recent trends and source attribution. *Geophysical Research Letters*, 47(1), e2019GL085866. <https://doi.org/10.1029/2019GL085866>
- Dix, B., Francoeur, C., Li, M., Serrano-Calvo, R., Levelt, P. F., Veefkind, J. P., et al. (2022). Quantifying NO_x emissions from U.S. oil and gas production regions using TROPOMI NO₂. *ACS Earth and Space Chemistry*, 6(2), 403–414. <https://doi.org/10.1021/acsearthspacechem.1c00387>
- Dix, B., Li, M., Roosenbrand, E., Francoeur, C., Brown, S. S., Gilman, J. B., et al. (2023). Sources of formaldehyde in U.S. oil and gas production regions. *ACS Earth and Space Chemistry*, 7(12), 2444–2457. <https://doi.org/10.1021/acsearthspacechem.3c00203>
- Dyson, J. E., Whalley, L. K., Slater, E. J., Woodward-Massey, R., Ye, C., Lee, J. D., et al. (2023). Impact of HO₂ aerosol uptake on radical levels and O₃ production during summertime in Beijing. *Atmospheric Chemistry and Physics*, 23(10), 5679–5697. <https://doi.org/10.5194/acp-23-5679-2023>
- Edwards, P. M., Brown, S. S., Roberts, J. M., Ahmadov, R., Banta, R. M., de Gouw, J. A., et al. (2014). High winter ozone pollution from carbonyl photolysis in an oil and gas basin. *Nature*, 514(7522), 351–354. <https://doi.org/10.1038/nature13767>
- Edwards, P. M., Young, C. J., Aikin, K., deGouw, J., Dubé, W. P., Geiger, F., et al. (2013). Ozone photochemistry in an oil and natural gas extraction region during winter: Simulations of a snow-free season in the Uintah Basin, Utah. *Atmospheric Chemistry and Physics*, 13(17), 8955–8971. <https://doi.org/10.5194/acp-13-8955-2013>
- Ericson, S., Engel-Cox, J., & Arent, D. (2019). *Approaches for integrating renewable energy technologies in oil and gas operations (Technical Report)*. Joint Institute for Strategic Energy Analysis.
- Fahey, D. W., Hübler, G., Parrish, D. D., Williams, E. J., Norton, R. B., Ridley, B. A., et al. (1986). Reactive nitrogen species in the troposphere: Measurements of NO, NO₂, HNO₃, particulate nitrate, peroxyacetyl nitrate (PAN), O₃, and total reactive odd nitrogen (NO_y) at Niwot Ridge, Colorado. *Journal of Geophysical Research*, 91(D9), 9781–9793. <https://doi.org/10.1029/JD091iD09p09781>
- Fedak, K. M., Good, N., Dahlke, J., Hecobian, A., Sullivan, A., Zhou, Y., et al. (2018). Chemical composition and emissions factors for cookstove startup (ignition) materials. *Environmental Science & Technology*, 52(16), 9505–9513. <https://doi.org/10.1021/acs.est.8b02218>
- Francoeur, C. B., McDonald, B. C., Gilman, J. B., Zarzana, K. J., Dix, B., Brown, S. S., et al. (2021). Quantifying methane and ozone precursor emissions from oil and gas production regions across the contiguous US. *Environmental Science & Technology*, 55(13), 9129–9139. <https://doi.org/10.1021/acs.est.0c07352>
- Gaudel, A., Cooper, O. R., Ancellet, G., Barret, B., Boynard, A., Burrows, J. P., et al. (2018). Tropospheric Ozone Assessment Report: Present-day distribution and trends of tropospheric ozone relevant to climate and global atmospheric chemistry model evaluation. *Elementa: Science of the Anthropocene*, 6, 39. <https://doi.org/10.1525/elementa.291>
- Gilman, J. B., Lerner, B. M., Kuster, W. C., & De Gouw, J. A. (2013). Source signature of volatile organic compounds from oil and natural gas operations in northeastern Colorado. *Environmental Science & Technology*, 47(3), 1297–1305. <https://doi.org/10.1021/es304119a>
- Gorchov Negron, A. M., McDonald, B. C., McKeen, S. A., Peischl, J., Ahmadov, R., De Gouw, J. A., et al. (2018). Development of a fuel-based oil and gas inventory of nitrogen oxides emissions. *Environmental Science & Technology*, 52(17), 10175–10185. <https://doi.org/10.1021/acs.est.8b02245>
- HIFLD. (2019). Oil and natural gas wells [Dataset]. Retrieved from <https://hifld-geoplatform.opendata.arcgis.com/datasets/oil-and-natural-gas-wells/explore>
- Ivatt, P. D., Evans, M. J., & Lewis, A. C. (2022). Suppression of surface ozone by an aerosol-inhibited photochemical ozone regime. *Nature Geoscience*, 15(7), 536–540. <https://doi.org/10.1038/s41561-022-00972-9>
- Jaffe, D. A., Ninneman, M., & Chan, H. C. (2022). NO_x and O₃ trends at U.S. non-attainment areas for 1995–2020: Influence of COVID-19 reductions and wildland fires on policy-relevant concentrations. *Journal of Geophysical Research: Atmospheres*, 127(11), e2021JD036385. <https://doi.org/10.1029/2021JD036385>

- Jenkin, M. E., Young, J. C., & Rickard, A. R. (2015). The MCM v3.3.1 degradation scheme for isoprene. *Atmospheric Chemistry and Physics*, 15(20), 11433–11459. <https://doi.org/10.5194/acp-15-11433-2015>
- Jin, X., & Holloway, T. (2015). Spatial and temporal variability of ozone sensitivity over China observed from the ozone monitoring instrument: Ozone sensitivity over China. *Journal of Geophysical Research: Atmospheres*, 120(14), 7229–7246. <https://doi.org/10.1002/2015JD023250>
- Kim, H., Park, R. J., Kim, S., Brune, W. H., Diskin, G. S., Fried, A., et al. (2022). Observed versus simulated OH reactivity during KORUS-AQ campaign: Implications for emission inventory and chemical environment in East Asia. *Elementa: Science of the Anthropocene*, 10(1), 00030. <https://doi.org/10.1525/elementa.2022.00030>
- Kleinman, L. I. (2005). The dependence of tropospheric ozone production rate on ozone precursors. *Atmospheric Environment*, 39(3), 575–586. <https://doi.org/10.1016/j.atmosenv.2004.08.047>
- Kleinman, L. I., Daum, P. H., Imre, D. G., Lee, J. H., Lee, Y.-N., Nunnermacker, L. J., et al. (2000). Ozone production in the New York City urban plume. *Journal of Geophysical Research*, 105(D11), 14495–14511. <https://doi.org/10.1029/2000JD900011>
- Kleinman, L. I., Springston, S. R., Daum, P. H., Weinstein-Lloyd, J., Alexander, M. L., Hubbe, J., et al. (2008). The time evolution of aerosol composition over the Mexico City Plateau. *Atmospheric Chemistry and Physics*, 8, 1559–1575. <https://doi.org/10.5194/acp-8-1559-2008>
- Kohut, R. (2007). Assessing the risk of foliar injury from ozone on vegetation in parks in the U.S. National Park Service's Vital Signs Network. *Environmental Pollution*, 149(3), 348–357. <https://doi.org/10.1016/j.envpol.2007.04.022>
- Kopplitz, S., Simon, H., Henderson, B., Liljegren, J., Tonnesen, G., Whitehill, A., & Wells, B. (2022). Changes in ozone chemical sensitivity in the United States from 2007 to 2016. *ACS Environmental Au*, 2(3), 206–222. <https://doi.org/10.1021/acsenvironau.1c00029>
- Kort, E. A., Smith, M. L., Murray, L. T., Gvakharia, A., Brandt, A. R., Peischl, J., et al. (2016). Fugitive emissions from the Bakken shale illustrate role of shale production in global ethane shift. *Geophysical Research Letters*, 43(9), 4617–4623. <https://doi.org/10.1002/2016GL068703>
- Koss, A. R., De Gouw, J., Warneke, C., Gilman, J. B., Lerner, B. M., Graus, M., et al. (2015). Photochemical aging of volatile organic compounds associated with oil and natural gas extraction in the Uintah Basin, UT, during a wintertime ozone formation event. *Atmospheric Chemistry and Physics*, 15(10), 5727–5741. <https://doi.org/10.5194/acp-15-5727-2015>
- Ku, I.-T., Zhou, Y., Hecobian, A., Benedict, K., Buck, B., Lachenmayer, E., et al. (2024). Air quality impacts from the development of unconventional oil and gas well pads: Air toxics and other volatile organic compounds. *Atmospheric Environment*, 317, 120187. <https://doi.org/10.1016/j.atmosenv.2023.120187>
- Lee, Y., Huey, L. G., Wang, Y., Qu, H., Zhang, R., Ji, Y., et al. (2021). Photochemistry of volatile organic compounds in the Yellow River Delta, China: Formation of O₃ and peroxyacyl nitrates. *Journal of Geophysical Research: Atmospheres*, 126(23), e2021JD035296. <https://doi.org/10.1029/2021JD035296>
- Li, S.-M., Leithead, A., Moussa, S. G., Liggio, J., Moran, M. D., Wang, D., et al. (2017). Differences between measured and reported volatile organic compound emissions from oil sands facilities in Alberta, Canada. *Proceedings of the National Academy of Sciences of the United States of America*, 114(19). <https://doi.org/10.1073/pnas.1617862114>
- Lindaas, J., Farmer, D. K., Pollack, I. B., Abeleira, A., Flocke, F., & Fischer, E. V. (2019). Acyl peroxy nitrates link oil and natural gas emissions to high ozone abundances in the Colorado Front Range during summer 2015. *Journal of Geophysical Research: Atmospheres*, 124(4), 2336–2350. <https://doi.org/10.1029/2018JD028825>
- Long, R. W., Whitehill, A., Habel, A., Urbanski, S., Halliday, H., Colón, M., et al. (2021). Comparison of ozone measurement methods in biomass burning smoke: An evaluation under field and laboratory conditions. *Atmospheric Measurement Techniques*, 14(3), 1783–1800. <https://doi.org/10.5194/amt-14-1783-2021>
- Lu, X., Jacob, D. J., Zhang, Y., Shen, L., Sulprizio, M. P., Maasakkers, J. D., et al. (2023). Observation-derived 2010–2019 trends in methane emissions and intensities from US oil and gas fields tied to activity metrics. *Proceedings of the National Academy of Sciences of the United States of America*, 120(17), e2217900120. <https://doi.org/10.1073/pnas.2217900120>
- Majid, A., Val Martin, M., Lamsal, L. N., & Duncan, B. N. (2017). A decade of changes in nitrogen oxides over regions of oil and natural gas activity in the United States. *Elementa: Science of the Anthropocene*, 5, 76. <https://doi.org/10.1525/elementa.259>
- Mao, J., Ren, X., Chen, S., Brune, W. H., Chen, Z., Martinez, M., et al. (2010). Atmospheric oxidation capacity in the summer of Houston 2006: Comparison with summer measurements in other metropolitan studies. *Atmospheric Environment*, 44(33), 4107–4115. <https://doi.org/10.1016/j.atmosenv.2009.01.013>
- Mayhew, A. W., Lee, B. H., Thornton, J. A., Bannan, T. J., Brean, J., Hopkins, J. R., et al. (2022). Evaluation of isoprene nitrate chemistry in detailed chemical mechanisms. *Atmospheric Chemistry and Physics*, 22(22), 14783–14798. <https://doi.org/10.5194/acp-22-14783-2022>
- McDuffie, E. E., Edwards, P. M., Gilman, J. B., Lerner, B. M., Dubé, W. P., Trainer, M., et al. (2016). Influence of oil and gas emissions on summertime ozone in the Colorado Northern Front Range: Colorado O&G and summertime ozone. *Journal of Geophysical Research: Atmospheres*, 121(14), 8712–8729. <https://doi.org/10.1002/2016JD025265>
- Monks, P. S., Archibald, A. T., Colette, A., Cooper, O., Coyle, M., Derwent, R., et al. (2015). Tropospheric ozone and its precursors from the urban to the global scale from air quality to short-lived climate forcer. *Atmospheric Chemistry and Physics*, 15(15), 8889–8973. <https://doi.org/10.5194/acp-15-8889-2015>
- Naimie, L. E., Sullivan, A. P., Benedict, K., Prenni, A. J., Sive, B., Schichtel, B. A., et al. (2022). PM_{2.5} in Carlsbad Caverns National Park: Composition, sources, and visibility impacts. *Journal of the Air & Waste Management Association*, 72(11), 1201–1218. <https://doi.org/10.1080/10962247.2022.2081634>
- NCEI. (2023). North American mesoscale forecast system [Dataset]. Retrieved from <https://www.ncei.noaa.gov/products/weather-climate-models/north-american-mesoscale>
- Ninneman, M., & Jaffe, D. A. (2021). The impact of wildfire smoke on ozone production in an urban area: Insights from field observations and photochemical box modeling. *Atmospheric Environment*, 267, 118764. <https://doi.org/10.1016/j.atmosenv.2021.118764>
- NPS. (2024). NPS gaseous pollutant & meteorological data access [Dataset]. Retrieved from <https://ard-request.air-resource.com/>
- Pan, D., Pollack, I. B., Sive, B. C., Marsavin, A., Naimie, L. E., Benedict, K. B., et al. (2023). Source characterization of volatile organic compounds at Carlsbad Caverns National Park. *Journal of the Air & Waste Management Association*, 73(12), 914–929. <https://doi.org/10.1080/10962247.2023.2266696>
- Pétron, G., Karion, A., Sweeney, C., Miller, B. R., Montzka, S. A., Frost, G. J., et al. (2014). A new look at methane and nonmethane hydrocarbon emissions from oil and natural gas operations in the Colorado Denver-Julesburg Basin. *Journal of Geophysical Research: Atmospheres*, 119(11), 6836–6852. <https://doi.org/10.1002/2013JD021272>
- Pollack, I. B., Pan, D., Marsavin, A., Cope, E. J., Juncosa Calahorrano, J., Naimie, L., et al. (2023). Observations of ozone, acyl peroxy nitrates, and their precursors during summer 2019 at Carlsbad Caverns National Park, New Mexico. *Journal of the Air & Waste Management Association*, 73(12), 951–968. <https://doi.org/10.1080/10962247.2023.2271436>
- Pozzer, A., Schultz, M. G., & Helmig, D. (2020). Impact of U.S. oil and natural gas emission increases on surface ozone is most pronounced in the Central United States. *Environmental Science & Technology*, 54(19), 12423–12433. <https://doi.org/10.1021/acs.est.9b06983>

- Prenni, A. J., Day, D. E., Evanowski-Cole, A. R., Sive, B. C., Hecobian, A., Zhou, Y., et al. (2016). Oil and gas impacts on air quality in federal lands in the Bakken region: An overview of the Bakken Air Quality Study and first results. *Atmospheric Chemistry and Physics*, 16(3), 1401–1416. <https://doi.org/10.5194/acp-16-1401-2016>
- Rickly, P. S., Coggon, M. M., Aikin, K. C., Alvarez, R. J., Baidar, S., Gilman, J. B., et al. (2023). Influence of wildfire on urban ozone: An observationally constrained box modeling study at a site in the Colorado Front Range. *Environmental Science & Technology*, 57(3), 1257–1267. <https://doi.org/10.1021/acs.est.2c06157>
- Robertson, A. M., Edie, R., Field, R. A., Lyon, D., McVay, R., Omara, M., et al. (2020). New Mexico Permian Basin measured well pad methane emissions are a factor of 5–9 times higher than U.S. EPA estimates. *Environmental Science & Technology*, 54(21), 13926–13934. <https://doi.org/10.1021/acs.est.0c02927>
- Sakamoto, Y., Sadanaga, Y., Li, J., Matsuoka, K., Takemura, M., Fujii, T., et al. (2019). Relative and absolute sensitivity analysis on ozone production in Tsukuba, a City in Japan. *Environmental Science & Technology*, 53(23), 13629–13635. <https://doi.org/10.1021/acs.est.9b03542>
- Seltzer, K. M., Murphy, B. N., Pennington, E. A., Allen, C., Talgo, K., & Pye, H. O. T. (2022). Volatile chemical product enhancements to criteria pollutants in the United States. *Environmental Science & Technology*, 56(11), 6905–6913. <https://doi.org/10.1021/acs.est.1c04298>
- Serrano-Calvo, R., Veeffkind, J. P., Dix, B., De Gouw, J., & Levelt, P. F. (2023). COVID-19 impact on the oil and gas industry NO₂ emissions: A case study of the Permian Basin. *Journal of Geophysical Research: Atmospheres*, 128(13), e2023JD038566. <https://doi.org/10.1029/2023JD038566>
- Sillman, S. (1999). The relation between ozone, NO_x and hydrocarbons in urban and polluted rural environments. *Atmospheric Environment*, 33(12), 1821–1845. [https://doi.org/10.1016/S1352-2310\(98\)00345-8](https://doi.org/10.1016/S1352-2310(98)00345-8)
- Sillman, S., & He, D. (2002). Some theoretical results concerning O₃-NO_x-VOC chemistry and NO_x-VOC indicators. *Journal of Geophysical Research*, 107(D22), 4659. <https://doi.org/10.1029/2001JD001123>
- Sillman, S., Logan, J. A., & Wofsy, S. C. (1990). The sensitivity of ozone to nitrogen oxides and hydrocarbons in regional ozone episodes. *Journal of Geophysical Research*, 95(D2), 1837–1851. <https://doi.org/10.1029/JD095iD02p01837>
- Sillman, S., & West, J. J. (2009). Reactive nitrogen in Mexico City and its relation to ozone-precursor sensitivity: Results from photochemical models. *Atmospheric Chemistry and Physics*, 9(9), 3477–3489. <https://doi.org/10.5194/acp-9-3477-2009>
- Simon, H., Reff, A., Wells, B., Xing, J., & Frank, N. (2015). Ozone trends across the United States over a period of decreasing NO_x and VOC emissions. *Environmental Science & Technology*, 49(1), 186–195. <https://doi.org/10.1021/es504514z>
- Sive, B. C., Zhou, Y., Troop, D., Wang, Y., Little, W. C., Wingenter, O. W., et al. (2005). Development of a cryogen-free concentration system for measurements of volatile organic compounds. *Analytical Chemistry*, 77(21), 6989–6998. <https://doi.org/10.1021/ac0506231>
- Song, H., Lu, K., Dong, H., Tan, Z., Chen, S., Zeng, L., & Zhang, Y. (2022). Reduced aerosol uptake of hydroperoxyl radical may increase the sensitivity of ozone production to volatile organic compounds. *Environmental Science and Technology Letters*, 9(1), 22–29. <https://doi.org/10.1021/acs.estlett.1c00893>
- Souri, A. H., Johnson, M. S., Wolfe, G. M., Crawford, J. H., Fried, A., Wisthaler, A., et al. (2023). Characterization of errors in satellite-based HCHO NO₂ tropospheric column ratios with respect to chemistry, column-to-PBL translation, spatial representation, and retrieval uncertainties. *Atmospheric Chemistry and Physics*, 23(3), 1963–1986. <https://doi.org/10.5194/acp-23-1963-2023>
- Stein, A. F., Draxler, R. R., Rolph, G. D., Stunder, B. J. B., Cohen, M. D., & Ngan, F. (2015). NOAA's HYSPLIT atmospheric transport and dispersion modeling system. *Bulletin of the American Meteorological Society*, 96(12), 2059–2077. <https://doi.org/10.1175/BAMS-D-14-00110.1>
- Strode, S. A., Rodriguez, J. M., Logan, J. A., Cooper, O. R., Witte, J. C., Lamsal, L. N., et al. (2015). Trends and variability in surface ozone over the United States. *Journal of Geophysical Research: Atmospheres*, 120(17), 9020–9042. <https://doi.org/10.1002/2014JD022784>
- Sullivan, A. P., Naimie, L. E., Benedict, K. B., Prenni, A. J., Sive, B. C., Fischer, E. V., et al. (2022). Carlsbad Caverns national park air quality study 2019 [Dataset]. *Mountain Scholar*. <https://doi.org/10.25675/10217235481>
- Swarthout, R. F., Russo, R. S., Zhou, Y., Hart, A. H., & Sive, B. C. (2013). Volatile organic compound distributions during the NACHTT campaign at the Boulder Atmospheric Observatory: Influence of urban and natural gas sources: Volatile organic compounds during NACHTT. *Journal of Geophysical Research: Atmospheres*, 118(18), 10614–10637. <https://doi.org/10.1002/jgrd.50722>
- Tzompa-Sosa, Z. A., & Fischer, E. V. (2021). Impacts of emissions of C₂-C₅ alkanes from the U.S. oil and gas sector on ozone and other secondary species. *Journal of Geophysical Research: Atmospheres*, 126(1), e2019JD031935. <https://doi.org/10.1029/2019JD031935>
- US EIA. (2016). Maps: Oil and gas exploration, resources, and production. Retrieved from <https://www.eia.gov/maps/maps.htm>
- US EIA. (2021). United States continued to lead global petroleum and natural gas production in 2020. Retrieved from <https://www.eia.gov/todayinenergy/detail.php?id=48756>
- US EIA. (2023). Drilling productivity report (Technical Report). Retrieved from <https://www.eia.gov/petroleum/drilling/>
- US EPA. (2023). Ozone trends. Retrieved from <https://www.epa.gov/air-trends/ozone-trends>
- Wang, P., Chen, Y., Hu, J., Zhang, H., & Ying, Q. (2019). Attribution of tropospheric ozone to NO_x and VOC emissions: Considering ozone formation in the transition regime. *Environmental Science & Technology*, 53(3), 1404–1412. <https://doi.org/10.1021/acs.est.8b05981>
- Wang, X., Hu, K., Hao, Y., Yin, Y., Xu, J., Li, Y., et al. (2024). Volatile organic compounds (VOCs) emission interferes with real-time regulatory monitoring of ozone in urban atmosphere. *Urban Climate*, 55, 101938. <https://doi.org/10.1016/j.uclim.2024.101938>
- Warneke, C., McKeen, S. A., De Gouw, J. A., Goldan, P. D., Kuster, W. C., Holloway, J. S., et al. (2007). Determination of urban volatile organic compound emission ratios and comparison with an emissions database. *Journal of Geophysical Research*, 112(D10), 2006JD007930. <https://doi.org/10.1029/2006JD007930>
- Wolfe, G. M., & Haskins, J., & SROBE. (2023). AirChem/F0AM: v4.2.2 [Software]. *Zenodo*. <https://doi.org/10.5281/zenodo.6984581>
- Wolfe, G. M., Marvin, M. R., Roberts, S. J., Travis, K. R., & Liao, J. (2016). The framework for 0-D atmospheric modeling (F0AM) v3.1. *Geoscientific Model Development*, 9(9), 3309–3319. <https://doi.org/10.5194/gmd-9-3309-2016>
- Xiong, Y., Chai, J., Mao, H., Mariscal, N., Yacovitch, T., Lerner, B., et al. (2023). Examining the summertime ozone formation regime in southeast Michigan using MOOSE ground-based HCHO/NO₂ measurements and F0AM box model. *Journal of Geophysical Research: Atmospheres*, 128(19), e2023JD038943. <https://doi.org/10.1029/2023JD038943>
- Xue, L. K., Wang, T., Guo, H., Blake, D. R., Tang, J., Zhang, X. C., et al. (2013). Sources and photochemistry of volatile organic compounds in the remote atmosphere of western China: Results from the Mt. Waliguan Observatory. *Atmospheric Chemistry and Physics*, 13(17), 8551–8567. <https://doi.org/10.5194/acp-13-8551-2013>
- Zare, A., Romer, P. S., Nguyen, T., Keutsch, F. N., Skog, K., & Cohen, R. C. (2018). A comprehensive organic nitrate chemistry: Insights into the lifetime of atmospheric organic nitrates. *Atmospheric Chemistry and Physics*, 18(20), 15419–15436. <https://doi.org/10.5194/acp-18-15419-2018>

References From the Supporting Information

- Atkinson, R., & Arey, J. (2003). Atmospheric degradation of volatile organic compounds. *Chemical Reviews*, 103(12), 4605–4638. <https://doi.org/10.1021/cr0206420>
- Atkinson, R., & Aschmann, S. M. (1984). Rate constants for the reactions of O₃ and OH radicals with a series of alkynes. *International Journal of Chemical Kinetics*, 16(3), 259–268. <https://doi.org/10.1002/kin.550160308>
- Dunne, E., Galbally, I. E., Cheng, M., Selleck, P., Molloy, S. B., & Lawson, S. J. (2018). Comparison of VOC measurements made by PTR-MS, adsorbent tubes–GC-FID-MS and DNPH derivatization–HPLC during the Sydney Particle Study, 2012: A contribution to the assessment of uncertainty in routine atmospheric VOC measurements. *Atmospheric Measurement Techniques*, 11(1), 141–159. <https://doi.org/10.5194/amt-11-141-2018>
- Finlayson-Pitts, B. J., & Pitts, J. N. J. (2000). *Chemistry of the upper and lower atmosphere*. Academic Press.
- Gelaro, R., McCarty, W., Suárez, M. J., Todling, R., Molod, A., Takacs, L., et al. (2017). The modern-era retrospective analysis for research and applications, version 2 (MERRA-2). *Journal of Climate*, 30(14), 5419–5454. <https://doi.org/10.1175/JCLI-D-16-0758.1>
- Hynes, A. J., & Wine, P. H. (1991). Kinetics and mechanism of the reaction of hydroxyl radicals with acetonitrile under atmospheric conditions. *The Journal of Physical Chemistry*, 95(3), 1232–1240. <https://doi.org/10.1021/j100156a037>
- Kaser, L., Patton, E. G., Pfister, G. G., Weinheimer, A. J., Montzka, D. D., Flocke, F., et al. (2017). The effect of entrainment through atmospheric boundary layer growth on observed and modeled surface ozone in the Colorado Front Range. *Journal of Geophysical Research: Atmospheres*, 122(11), 6075–6093. <https://doi.org/10.1002/2016JD026245>
- Lin, J., Youn, D., Liang, X., & Wuebbles, D. (2008). Global model simulation of summertime U.S. ozone diurnal cycle and its sensitivity to PBL mixing, spatial resolution, and emissions. *Atmospheric Environment*, 42(36), 8470–8483. <https://doi.org/10.1016/j.atmosenv.2008.08.012>
- Mao, J., Fan, S., Jacob, D. J., & Travis, K. R. (2013). Radical loss in the atmosphere from Cu-Fe redox coupling in aerosols. *Atmospheric Chemistry and Physics*, 13(2), 509–519. <https://doi.org/10.5194/acp-13-509-2013>
- Mouat, A. P., Siegel, Z. A., & Kaiser, J. (2023). Evaluation of Aeris MIRA, Picarro CRDS G2307, and DNPH-based sampling for long-term formaldehyde monitoring efforts. *EGU sphere*. <https://doi.org/10.5194/egusphere-2023-703>
- Orkin, V. L., Khamaganov, V. G., Kozlov, S. N., & Kurylo, M. J. (2013). Measurements of rate constants for the OH reactions with bromoform (CHBr₃), CHBr₂Cl, CHBrCl₂, and epichlorohydrin (C₃H₅ClO). *The Journal of Physical Chemistry A*, 117(18), 3809–3818. <https://doi.org/10.1021/jp3128753>
- Orlando, J. J., Tyndall, G. S., Wallington, T. J., & Dill, M. (1996). Atmospheric chemistry of CH₂Br₂: Rate coefficients for its reaction with Cl atoms and OH and the chemistry of the CHBr₂O radical. *International Journal of Chemical Kinetics*, 28(6), 433–442. [https://doi.org/10.1002/\(SICI\)1097-4601\(1996\)28:6<433::AID-KIN5>3.0.CO;2-W](https://doi.org/10.1002/(SICI)1097-4601(1996)28:6<433::AID-KIN5>3.0.CO;2-W)
- Pelgrum, H., Schmugge, T., Rango, A., Ritchie, J., & Kustas, B. (2000). Length-scale analysis of surface albedo, temperature, and normalized difference vegetation index in desert grassland. *Water Resources Research*, 36(7), 1757–1765. <https://doi.org/10.1029/2000WR900028>
- Shaw, J. T., Rickard, A. R., Newland, M. J., & Dillon, T. J. (2020). Rate coefficients for reactions of OH with aromatic and aliphatic volatile organic compounds determined by the multivariate relative rate technique. *Atmospheric Chemistry and Physics*, 20(16), 9725–9736. <https://doi.org/10.5194/acp-20-9725-2020>
- Sprengnether, M. M., Demerjian, K. L., Dransfield, T. J., Clarke, J. S., Anderson, J. G., & Donahue, N. M. (2009). Rate constants of nine C₆C₉ alkanes with OH from 230 to 379 K: Chemical tracers for [OH]. *The Journal of Physical Chemistry A*, 113(17), 5030–5038. <https://doi.org/10.1021/jp810412m>
- Stockwell, W. R., Kirchner, F., Kuhn, M., & Seefeld, S. (1997). A new mechanism for regional atmospheric chemistry modeling. *Journal of Geophysical Research*, 102(D22), 25847–25879. <https://doi.org/10.1029/97JD00849>
- Taylor, P. H., Jiang, Z., & Dellinger, B. (1993). Determination of the gas-phase reactivity of hydroxyl with chlorinated methanes at high temperature: Effects of laser/thermal photochemistry. *International Journal of Chemical Kinetics*, 25(1), 9–23. <https://doi.org/10.1002/kin.550250103>
- Tichenor, L. B., El-Sinawi, A., Yamada, T., Taylor, P. H., Peng, J., Hu, X., & Marshall, P. (2001). Kinetic studies of the reaction of hydroxyl radicals with trichloroethylene and tetrachloroethylene. *Chemosphere*, 42(5–7), 571–577. [https://doi.org/10.1016/S0045-6535\(00\)00229-0](https://doi.org/10.1016/S0045-6535(00)00229-0)
- Wang, W., Yuan, B., Peng, Y., Su, H., Cheng, Y., Yang, S., et al. (2022). Direct observations indicate photodegradable oxygenated volatile organic compounds (OVOCs) as larger contributors to radicals and ozone production in the atmosphere. *Atmospheric Chemistry and Physics*, 22(6), 4117–4128. <https://doi.org/10.5194/acp-22-4117-2022>
- Wilson, E. W., Hamilton, W. A., Kennington, H. R., Evans, B., Scott, N. W., & DeMore, W. B. (2006). Measurement and estimation of rate constants for the reactions of hydroxyl radical with several alkanes and cycloalkanes. *The Journal of Physical Chemistry A*, 110(10), 3593–3604. <https://doi.org/10.1021/jp055841c>
- Xu, W., Zhang, G., Wang, Y., Tong, S., Zhang, W., Ma, Z., et al. (2021). Aerosol promotes peroxyacetyl nitrate formation during winter in the North China Plain. *Environmental Science & Technology*, 55(6), 3568–3581. <https://doi.org/10.1021/acs.est.0c08157>